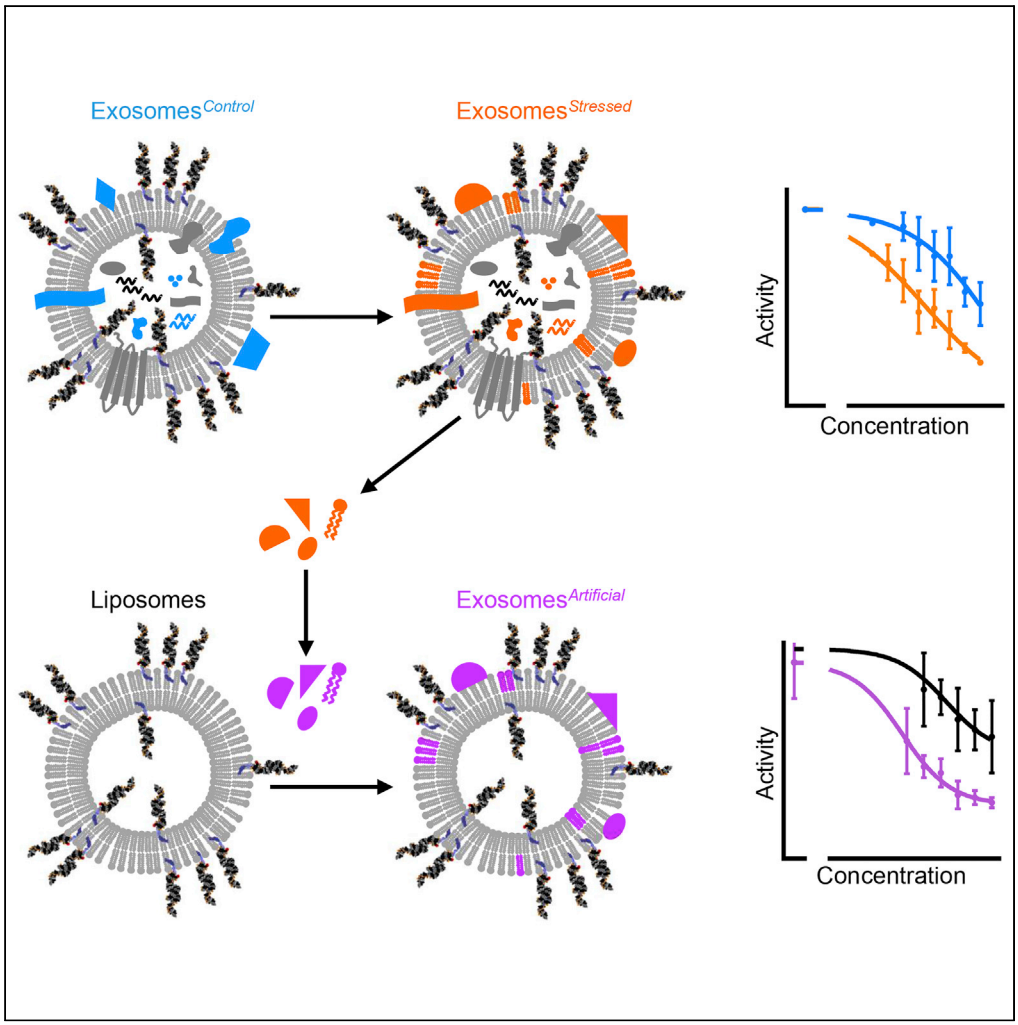
iScience

CellPress

Article

Serum Deprivation of Mesenchymal Stem Cells Improves Exosome Activity and Alters Lipid and Protein Composition



Reka Agnes Haraszti, Rachael Miller, Michelle L. Dubuke, ..., Marian DiFiglia, Neil Aronin, Anastasia Khvorova

rharaszti@gmail.com (R.A.H.)
neil.aronin@umassmed.edu (N.A.)
anastasia.khvorova@umassmed.edu (A.K.)

HIGHLIGHTS

Source cell stress augments exosome activity but reduces microvesicle activity

Source cell stress alters exosome lipid and protein composition

DSP, Rab7, AHSG an dilysocardiolipin enhances exosome activity

Haraszti et al., iScience *16*, 230–241
June 28, 2019 © 2019 The Author(s).
https://doi.org/10.1016/j.isci.2019.05.029

iScience

CellPress

Article

Serum Deprivation of Mesenchymal Stem Cells Improves Exosome Activity and Alters Lipid and Protein Composition

Reka Agnes Haraszti,[1,8,9,*] Rachael Miller,[1,2] Michelle L. Dubuke,[3] Hannah E. Rockwell,[4] Andrew H. Coles,[1] Ellen Sapp,[5] Marie-Cecile Didiot,[1] Dimas Echeverria,[1] Matteo Stoppato,[6] Yves Y. Sere,[6] John Leszyk,[3] Julia F. Alterman,[1] Bruno M.D.C. Godinho,[1] Matthew R. Hassler,[1] Justice McDaniel,[4] Niven R. Narain,[4] Rachel Wollacott,[6] Yang Wang,[6] Scott A. Shaffer,[3] Michael A. Kiebish,[4] Marian DiFiglia,[5] Neil Aronin,[1,2,*] and Anastasia Khvorova[1,7,*]

SUMMARY

Exosomes can serve as delivery vehicles for advanced therapeutics. The components necessary and sufficient to support exosomal delivery have not been established. Here we connect biochemical composition and activity of exosomes to optimize exosome-mediated delivery of small interfering RNAs (siRNAs). This information is used to create effective artificial exosomes. We show that serum-deprived mesenchymal stem cells produce exosomes up to 22-fold more effective at delivering siRNAs to neurons than exosomes derived from control cells. Proteinase treatment of exosomes stops siRNA transfer, indicating that surface proteins on exosomes are involved in trafficking. Proteomic and lipidomic analyses show that exosomes derived in serum-deprived conditions are enriched in six protein pathways and one lipid class, dilysocardiolipin. Inspired by these findings, we engineer an "artificial exosome," in which the incorporation of one lipid (dilysocardiolipin) and three proteins (Rab7, Desmoplakin, and AHSG) into conventional neutral liposomes produces vesicles that mimic cargo delivering activity of natural exosomes.

INTRODUCTION

Extracellular vesicles (EVs), including exosomes (small EVs) and microvesicles (large EVs), transfer molecules, such as therapeutic RNAs (Lener et al., 2015; Kramer-Albers, 2017; Kamerkar et al., 2017), to induce phenotype change in recipient cells (Valadi et al., 2007; Zomer et al., 2015; Fruhbeis et al., 2013; Monguio-Tortajada et al., 2017; Zhang et al., 2018). The following critical issues have impeded the use of exosomes for clinical applications: (1) production of exosomes from cells is tedious, has low yield, and is difficult to control; (2) the essential components of active exosomes are not established; and (3) the fundamental mechanisms of exosomal delivery need to be clarified to produce artificial exosomes in bulk. We optimized conditions to improve the delivery of exosomal cargo (small interfering RNA [siRNAs]) and used these optimized exosomes to find molecules that may affect exosomal activity. We constructed artificial exosomes inspired by these findings. Our strategy aims to substitute natural exosomes with artificial exosomes appropriate for large-scale production.

Cellular stress increases the activity of EVs (Han et al., 2018; Mleczko et al., 2018; Guitart et al., 2016), possibly by altering their protein (Xie et al., 2018; Guitart et al., 2016; Sun et al., 2014; Li et al., 2015) and RNA composition (King et al., 2012; Pope and Lasser, 2013). Therefore relating the change in composition of EVs to the change in their activity under stressed and control conditions can establish a composition-activity relationship. Serum deprivation is a common means of inducing cellular stress (Oskowitz et al., 2011), is widely used in extracellular vesicle production, and has been found to alter EV number (Aubertin et al., 2016; Sun et al., 2014; Taverna et al., 2003), activity (Sun et al., 2014; Oskowitz et al., 2011; Taverna et al., 2003), and composition (Kowal et al., 2016; Li et al., 2015). Surface (Sun et al., 2014) and intravesicular proteins (Taverna et al., 2003) have been linked to improved EV activity upon serum deprivation. We speculated that the membrane composition (proteins and lipids) of EVs is responsible for EV intercellular trafficking activity. We showed that upon serum deprivation, producer cells release exosomes that are more efficient at delivering siRNAs to neurons (a model for intercellular trafficking). This activity change was accompanied by substantial protein and lipid composition changes. We then screened several proteins and lipids, which were enriched in stressed exosomes, for enhancement in

[1]RNA Therapeutics Institute, University of Massachusetts Medical School, Worcester, MA, USA

[2]Department of Medicine, University of Massachusetts Medical School, Worcester, MA, USA

[3]Mass Spectrometry Facility, Biochemistry and Molecular Pharmacology, University of Massachusetts Medical School, Shrewsbury, MA, USA

[4]BERG LLC, Framingham, MA, USA

[5]Mass General Institute for Neurodegenerative Disease, Boston, MA, USA

[6]MassBiologics, Boston, MA, USA

[7]Program in Molecular Medicine, University of Massachusetts Medical School, Worcester, MA, USA

[8]Present address: Universitätklinikum Tübingen, Innere Medizin 2, Otfried-Müller Str. 10., 72076 Tübingen, Germany

[9]Lead Contact

*Correspondence: rharaszti@gmail.com (R.A.H.), neil.aronin@umassmed.edu (N.A.), anastasia.khvorova@umassmed.edu (A.K.)

https://doi.org/10.1016/j.isci.2019.05.029

 © 2019 The Author(s).
This is an open access article under the CC BY-NC-ND license (http://creativecommons.org/licenses/by-nc-nd/4.0/).

vesicle-mediated siRNA delivery to neurons. Subsequently we combined a candidate lipid (dilysocardiolipin) and three candidate proteins (Rab7, AHSG, and Desmoplakin) from the screen into liposomes to construct "artificial exosomes." These artificial exosomes mimicked the siRNA delivery activity of natural stressed exosomes both *in vitro* and *in vivo*.

RESULTS

Characterization of Extracellular Vesicles Produced from Control and Serum-Deprived Mesenchymal Stem Cells

We incubated mesenchymal stem cells derived from umbilical cord, adipose tissue, and bone marrow in either the recommended stem cell medium depleted of EVs (*Control*) or serum-free RPMI medium for 24 h (*Stressed*). We used differential ultracentrifugation to generate two EV populations, small and large EVs, enriched based on their sedimentation properties (Thery et al., 2006). We refer to the EVs from the 10,000 × *g* pellet as microvesicles and EVs from the 100,000 × *g* pellet as exosomes. Throughout this study we compare stressed conditions with control conditions within the same sample type: stressed cells versus control cells, microvesicles from stressed versus from control cells, and exosomes from stressed versus from control cells.

Mesenchymal stem cells tolerated serum deprivation for up to 4 days (Figure S1A) without loss of viability. EVs showed homogeneous size distribution (Figure S1B). Exosomes and microvesicles isolated from both the control and stressed (serum deprived for 24 h) conditions displayed positive protein markers and were devoid of negative protein markers of EVs (Figure S1C) and appeared as lipid bilayer-surrounded vesicles on transmission electron microscopy (Figure S1D). Serum deprivation did not affect the exosome yield from umbilical cord-derived cells ($p = 0.3$), but significantly decreased the exosome yield from both adipose- and bone marrow-derived cells (6-fold, $p = 0.04$, and 10-fold, $p = 0.002$, respectively, Figure S2A). Serum deprivation did not alter the amount of microvesicles (Figure S2B). Exosomes derived from umbilical cord mesenchymal stem cells were slightly larger than exosomes from either adipose tissue or bone marrow cells (142 ± 14 nm, 110 ± 19 nm, and 117 ± 10 nm, respectively). Serum deprivation did not affect EV size (Figures S2C and S2D). Protein-to-particle ratio varied substantially between vesicles from different sources and was affected by serum deprivation for some EV populations (Figures S2E and S2F). Umbilical cord-derived exosomes had the lowest protein-to-particle ratio, which remained unchanged upon serum deprivation (Figures S2E and S2F).

Serum Deprivation of Mesenchymal Stem Cells Improves Exosome Activity but Impairs Microvesicle Activity

Extracellular vesicles transport RNA between cells (Valadi et al., 2007; Zomer et al., 2015; Yang et al., 2017). We previously have shown that exosomes can productively transfer loaded cholesterol-conjugated siRNAs to neurons (Didiot et al., 2016). We loaded *Huntingtin*-targeting, cholesterol-conjugated siRNA (Alterman et al., 2015) to exosomes and treated primary neurons as a model for exosome trafficking. We evaluated the rates of exosome uptake to neurons using confocal microscopy and quantified the level of guide strand accumulation and target mRNA silencing in neurons.

First, exosomes isolated from serum-deprived cells ($Exosomes^{Stressed}$) could be loaded with equal amount of siRNA as $Exosomes^{Control}$ (Figure S3). Second, $Exosomes^{Stressed}$ delivered more siRNA to target neurons than $Exosomes^{Control}$ across all mesenchymal stem cell origins tested (Figures 1A–1C). Third, when loaded with fluorescently labeled siRNA, $Exosomes^{Stressed}$ showed an approximately 2-fold faster neuronal uptake kinetic (half-time 1.7 h versus 3.8 h, $p < 0.0001$) (Figures S4A and S4B). Finally, siRNA-containing $Exosomes^{Stressed}$ were 5- to 22-fold more efficient at inducing *Huntingtin* mRNA silencing than $Exosomes^{Control}$ (Figures 1D–1F). A similar effect was observed with siRNAs targeting *Ppib* mRNA (Figure S4C).

Stress-dependent enhancement in activity was characteristic of exosomes and not of microvesicles, where serum deprivation impaired activity (Figures 1A–1F). These data pointed toward specific characteristics between exosomes and microvesicles that may be related to different vesicle trafficking: protein composition (Haraszti et al., 2016; Kowal et al., 2016).

Serum Deprivation of Mesenchymal Stem Cells Substantially Alters Protein Composition of Exosomes

To evaluate serum deprivation-induced changes in the protein composition of exosomes, we performed liquid chromatography-tandem mass spectrometry (LC-MS/MS) proteomic analysis. We collected data

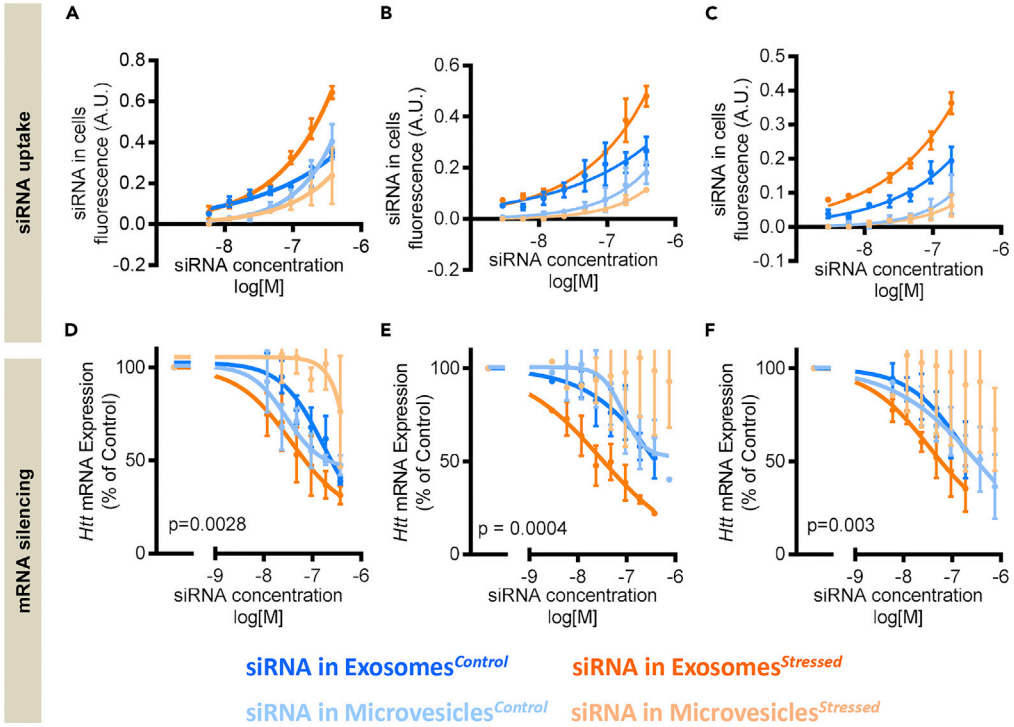


Figure 1. Serum Deprivation of Mesenchymal Stem Cells Improves Exosome Activity but Impairs Microvesicle Activity

Primary neurons were treated with fluorescent siRNA-containing exosomes or microvesicles derived from control or stressed (serum deprived) cells. After 7 days of incubation, siRNA levels and target mRNA levels were quantified in neurons. mRNA levels were normalized to housekeeping gene and to untreated control. N = 3, mean ± SEM, curves were compared using two-way ANOVA.

(A–C) Uptake of siRNA into neurons delivered via exosomes and microvesicle.

(D–F) mRNA silencing induced by treatment of siRNA-containing exosomes and microvesicles.

(A and D) EVs enriched from umbilical cord-derived mesenchymal stem cells. (B and E) EVs enriched from adipose tissue-derived mesenchymal stem cells. (C and F) EVs enriched from bone marrow-derived mesenchymal stem cells.

from three independent repeats of (1) control or serum-deprived mesenchymal stem cells (derived from umbilical cord, adipose tissue, or bone marrow), (2) microvesicles from control or serum-deprived cells, and (3) exosomes from control or serum-deprived cells.

As expected, serum deprivation had a profound effect on the proteome of cells, microvesicles, and exosomes, consistent in biological replicates (Figures 2A–2C and S5–S8). Protein composition differed substantially between exosomes and microvesicles (Figures S5–S8). Proteins enriched in stressed exosomes were either unchanged or depleted in corresponding microvesicles and source cells (Figures S5–S8 and 2D–2F).

Gene Ontology analysis showed enrichment of extracellular exosome, proteasome, membrane, desmosome, cell-cell adhesion, ribosome, and Golgi protein pathways in Exosomes^{Stressed} fractions throughout all cell sources tested (Figures 2G–2I). We hypothesized that proteins involved in membrane, desmosome, and cell-cell adhesion may be related to vesicle trafficking. In addition, categories frequently found in exosomes (multivesicular body, endosome, histone, tetraspanins) as well as categories non-canonical to exosomes (endoplasmic reticulum [ER], ER-to-Golgi transport, and chaperone proteins) were enriched in Exosomes^{Stressed} derived from at least two of three cell sources tested (Figures 2G–2I).

Several Proteins Enriched in Stressed Exosomes Contribute to Improved siRNA Transfer to Neurons

Altered protein composition may explain the enhanced activity of Exosomes^{Stressed}. Proteinase K treatment (degrades surface proteins) impaired the exosome-mediated siRNA transfer and resulted in less *Huntingtin*

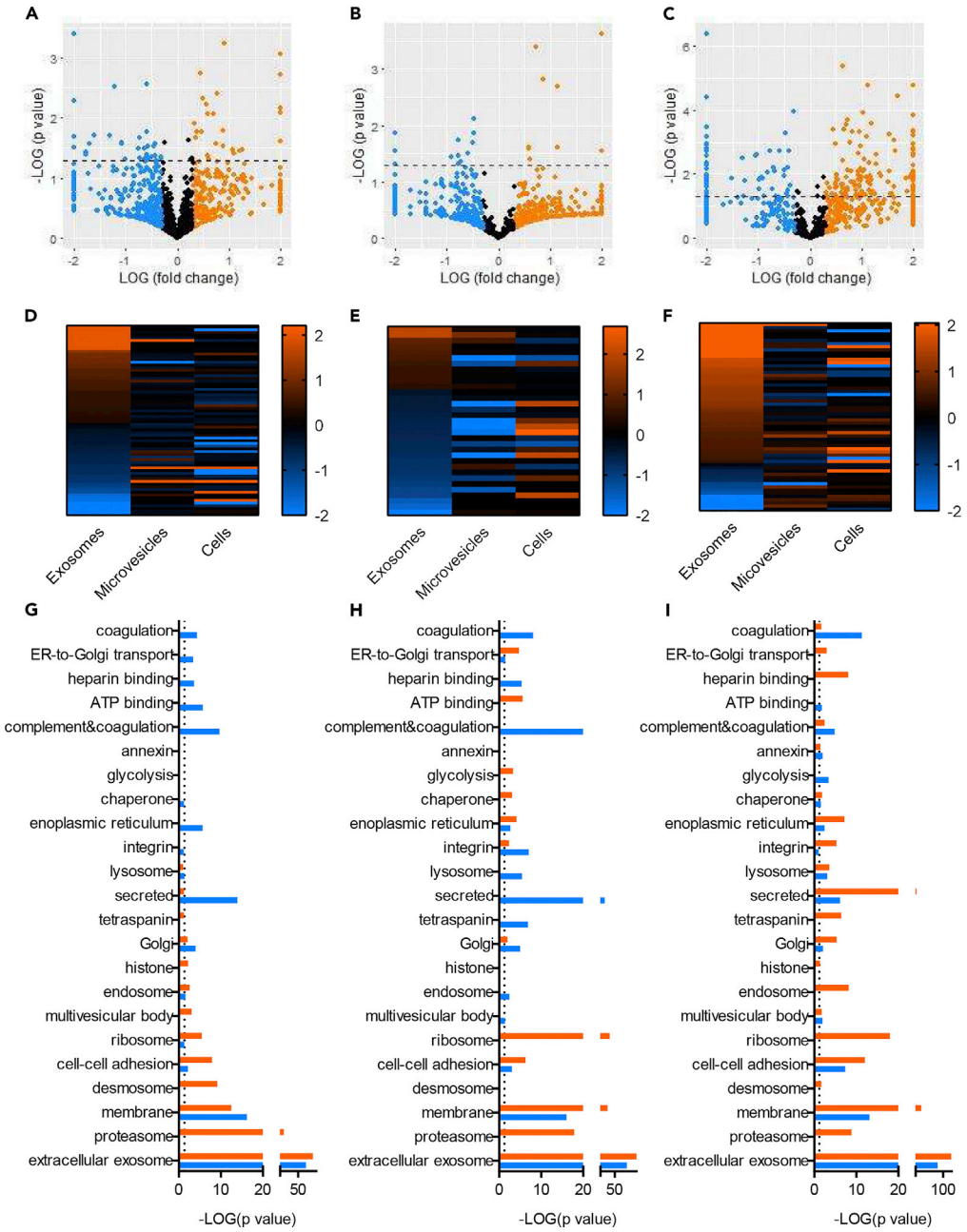


Figure 2. Serum Deprivation of Source Cells Alters Protein Content of Released Exosomes

Exosomes, microvesicles, and cells derived from control conditions or stress conditions (serum deprivation) underwent liquid chromatography-MS/MS proteomics analysis. N = 3 biological replicates were analyzed and label-free quantification carried out using intensity-based absolute quantification method.

(A–C) Volcano plots of proteins detected in exosome. Orange dots represent proteins enriched at least 2-fold in $Exosomes^{Stressed}$, and blue dots represent proteins enriched at least 2-fold in $Exosomes^{Control}$. Dashed line marks the threshold of significance ($p = 0.05$, t test with Benjamini-Hochberg correction for multiple comparison). Proteins above the dashed line significantly differ between $Exosomes^{Stressed}$ and $Exosomes^{Control}$. Proteins detected in one group and absent in the other group were arbitrarily assigned a fold change of 20 or -20.

(D–F) Heatmaps of proteins different ($p < 0.1$) in $Exosomes^{Stressed}$ versus $Exosomes^{Control}$. Orange represents enrichment in stressed conditions versus control conditions ($Exosomes^{Stressed}$ versus $Exosomes^{Control}$, $Microvesicles^{Stressed}$ versus $Microvesicles^{Control}$, and $Cells^{Stressed}$ versus $Cells^{Control}$), whereas blue represents enrichment in control conditions versus stress conditions.

Figure 2. *Continued*

(G–I) Gene Ontology analysis of proteins at least 2-fold enriched in Exosomes^{Stressed} or Exosomes^{Control} (e.g., proteins labeled orange or blue in panels A–C).

(A, D, and G) Umbilical cord-derived mesenchymal stem cells. (B, E, and H) Adipose tissue-derived mesenchymal stem cells. (C, F, and I) Bone marrow-derived mesenchymal stem cells.

silencing (Figures 3A and 3B), confirming that exosomes' surface proteins are essential for the delivery of cargo into neurons. The difference in the activity of Exosomes^{Stressed} over Exosomes^{Control} is not related to potential inhibition by serum proteins present, as incubation with serum-containing (EV-depleted) media had no effect on Exosomes^{Stressed} activity (Figure 3A).

To establish a protein composition-activity relationship in exosomes, we selected proteins that (1) have an established role in vesicle trafficking or membrane adhesion and (2) were enriched in stressed exosomes derived from at least two of three mesenchymal stem cell sources. Based on these criteria, the shortlist included proteins from endosomal pathways (Rab5 and Rab7; Kummel and Ungermann, 2014), plasma membrane budding (ARRDC1; Nabhan et al., 2012), secreted proteins interacting with membranes (dermcidin; Paulmann et al., 2012), desmosome (Desmocollin, Desmoplakin; Delva et al., 2009), and nucleo-extracellular shuttles (AHSG and histone 1; Watson et al., 2012) (Figure 3C). AHSG has been reported to shuttle histones from the nucleus to exosomes (Watson et al., 2012) and was consistently enriched in stressed cells (not present in EVs) (Figure 3C), whereas histones were specifically enriched in stressed exosomes (Figures 2G–2I and 3C).

Purified proteins were chemically palmitoylated and co-incubated with neutral liposomes (dioleoyl-phosphatidylcholine: cholesterol, 7:3) to promote association with the liposome membrane. Palmitoylation has been reported as a strategy to enrich proteins associated with exosomal membranes (Lai et al., 2015). Incorporation of Rab7, Desmoplakin, and AHSG improved liposome-mediated siRNA transfer to neurons and improved *Huntingtin* mRNA silencing ($p < 0.0001$ two-way ANOVA, Figure 3D). Incorporation of Rab5, Desmocollin, ARRDC1, Dermcidin, and histone 1 had no effect (Figure 3D). Thus incorporation of at least three candidate proteins from the proteomic analysis to the liposome surface affected the efficiency of vesicle transfer to neurons.

Dilysocardiolipin Enrichment in Stressed Exosomes Contributes to Improved Trafficking to Neurons

Membrane composition is a likely contributor to the enhanced trafficking activity of stressed exosomes. Membrane trafficking is regulated by both proteins and lipids (Ikonen, 2001; Huijbregts et al., 2000). To evaluate the effect of serum deprivation on the lipid composition of exosomes, we performed MS/MS^{ALL} lipidomic analysis. Among all lipid classes detected, only cardiolipins showed significant enrichment in exosomes derived from serum-deprived cells ($p = 0.004$, two-way ANOVA) (Figures 4A and S8A). Similar to protein enrichment, cardiolipin enrichment was specific to stressed exosomes and did not occur in corresponding cells and microvesicles (Figure 4A). In addition, we have observed a modest but statistically significant enrichment in unsaturated and long-tailed cardiolipins in stressed exosomes (Figures S8B and S8C).

Cardiolipin is a diphosphatidylglycerol lipid with four fatty acid tails (Figure 4B). Hydrolytic removal of one or two fatty acid tails results in the formation of monolysocardiolipin (Figure 4C) or dilysocardiolipin (Figure 4D), known intermediates in cardiolipin remodeling (Cao et al., 2004). Cardiolipin remodeling has been associated with highly curved membranes (Schlame et al., 2012).

Among different cardiolipin subclasses, dilysocardiolipins showed the highest enrichment in stressed exosomes (16-fold, $p < 0.0001$), followed by intact cardiolipins (9-fold, $p < 0.0001$) and monolysocardiolipins (6-fold, $p < 0.0001$) (Figure 4E), compared with control exosomes. Cardiolipin subclass enrichment was specific to stressed exosomes and was not observed in corresponding microvesicles and cells (Figure 4E).

To test whether cardiolipins play a role in vesicle trafficking to neurons, we incorporated intact cardiolipin, monolysocardiolipin, or dilysocardiolipin (30% of total lipid amount) in conventional liposomes (dioleoyl-phosphatidylcholine, cholesterol). Incorporation of dilysocardiolipin, but not other variants, into liposomes

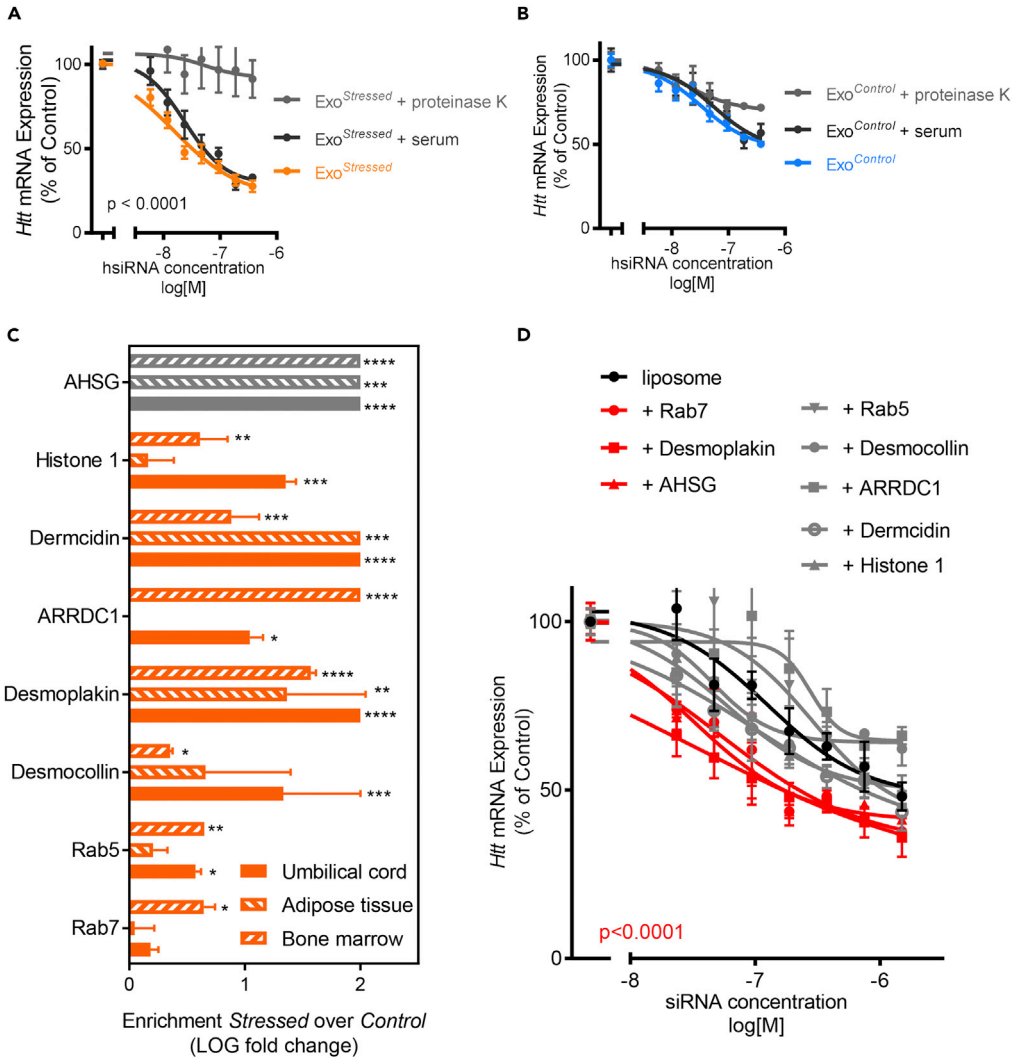


Figure 3. Proteins Enriched in Stressed Exosomes Contribute to Improved siRNA Transfer to Neurons

(A and B) Exosomes were enriched from serum-starved (A) or control (B) umbilical cord-derived mesenchymal stem cells and either not further treated or treated with proteinase K or EV-depleted serum-containing medium (serum). Primary neurons were then treated with the above exosome variants containing siRNAs, and mRNA levels in neurons were quantified after 7 days of incubation. N = 5, mean ± SEM, curves compared using two-way ANOVA.

(C) Enrichment of selected proteins in Exosomes^{Stressed} versus Exosomes^{Control} (orange) or in Cells^{Stressed} versus Cells^{Control} (gray). Proteins detected in stressed conditions but absent in control conditions were arbitrarily assigned the fold change of 20. N = 3, mean ± SEM. Two-way ANOVA, ****p < 0.0001, ***p < 0.001, **p < 0.01, *p < 0.05.

(D) Primary neurons were treated with siRNA containing liposomes alone or liposomes incorporating purified proteins from (C), and target mRNA levels in neurons were quantified after 7 days of incubation. N = 4, mean ± SEM, two-way ANOVA.

improved siRNA transfer to neurons and resulted in enhanced *Huntingtin* silencing (p = 0.007, two-way ANOVA) (Figure 4F). Thus dilysocardiolipin enrichment in stressed exosomes might be a contributing factor to enhanced neuronal uptake.

Artificial Exosomes Are Equally Active at siRNA Delivery as Natural Exosomes *In Vitro* and *In Vivo*

Having identified three proteins and one lipid class to be enriched in Exosomes^{Stressed} and improve vesicle uptake into neurons, we explored whether we can engineer an artificial exosome displaying similar activity

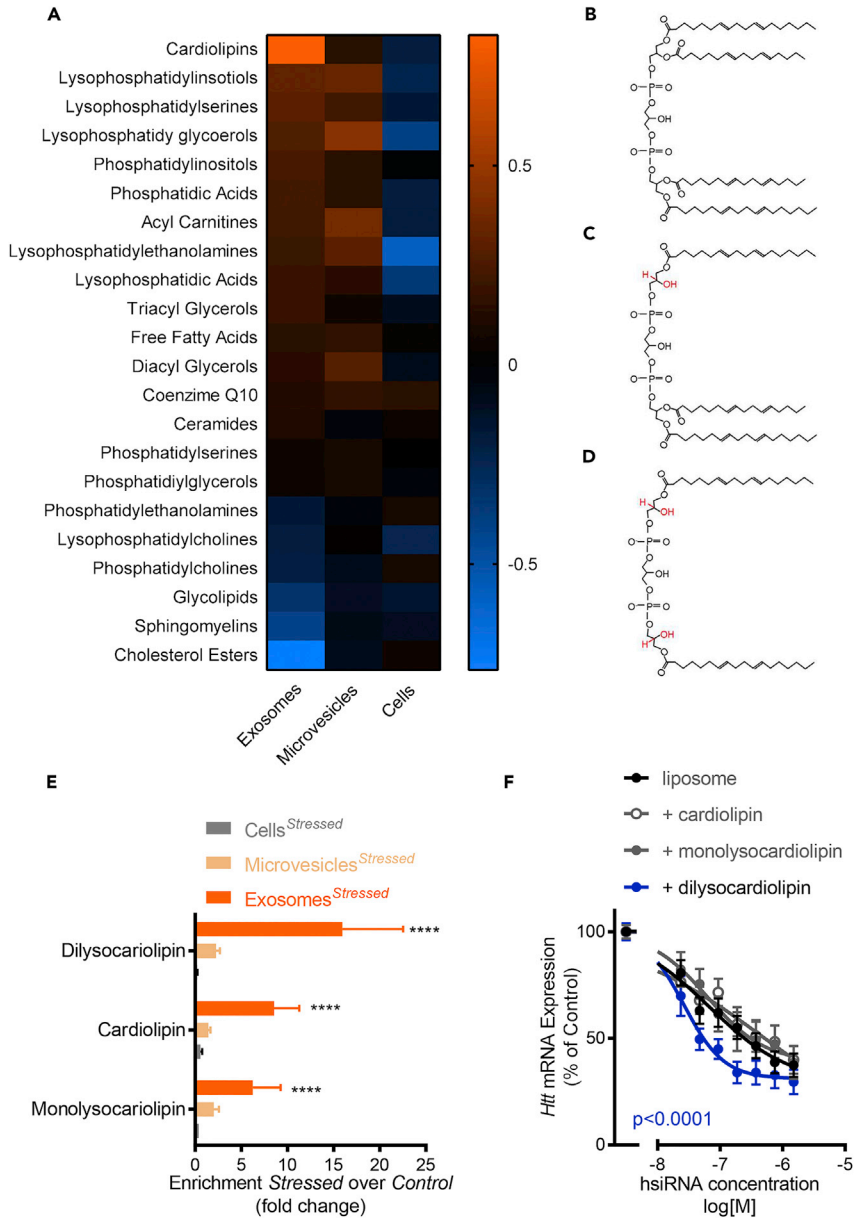


Figure 4. Dilysocardiolipin Enrichment in Stressed Exosomes Contributes to Improved Trafficking to Neurons

Exosomes purified from umbilical cord-derived mesenchymal stem cells under control conditions or stress conditions (serum deprivation) underwent MS/MS^{ALL} lipidomics analysis. N = 2–5 biological replicates were analyzed per group.

(A) Heatmap of lipid classes in stressed conditions versus control conditions. Orange represents enrichment in Exosomes^{Stressed} versus Exosomes^{Control}, Microvesicles^{Stressed} versus Microvesicles^{Control}, and Cells^{Stressed} versus Cells^{Control}, whereas blue represents enrichment in control conditions versus stress conditions.

(B) Scheme of cardiolipin. Length and saturation of fatty acid tails depicted is representative only and varies between natural cardiolipin species.

(C) Scheme of monolysocardiolipin. Differences to cardiolipin are shown in red. Length and saturation of fatty acid tails depicted are representative only and vary between natural monolysocardiolipin species.

(D) Scheme of dilysocardiolipin. Differences to cardiolipin are shown in red. Length and saturation of fatty acid tails depicted are representative only and vary between natural dilysocardiolipin species.

(E) Enrichment of cardiolipin subclasses from (B–D) in Exosomes^{Stressed} versus Exosomes^{Control} (dark orange), Microvesicles^{Stressed} versus Microvesicles^{Control} (light orange), and in Cells^{Stressed} versus Cells^{Control} (gray). Two-way ANOVA, ****$p < 0.0001$. N = 3, mean ± SEM.

(F) Primary neurons were treated with siRNA containing liposomes alone or liposomes incorporating lipids from panel (E) and target mRNA levels in neurons quantified after 7 days of incubation. N = 4, mean ± SEM, two-way ANOVA.

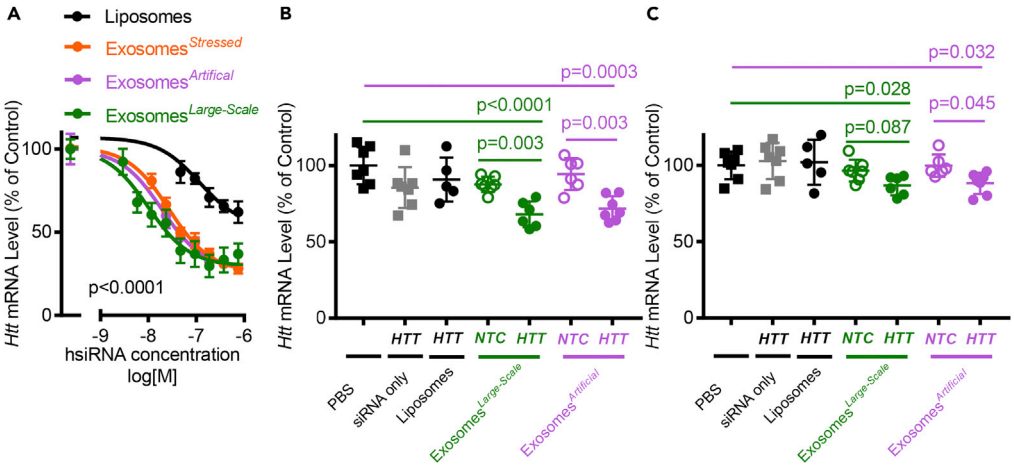


Figure 5. Artificial Exosomes Recapitulate the Activity of Stressed Exosomes

(A) Primary neurons were treated with siRNA containing Exosomes^{Stressed}, Exosome$^{Large\text{-}Scale}$, or Exosomes^{Articial} and target mRNA levels in neurons quantified after 7 days of incubation. Exosomes^{Stressed} and Exosome$^{Large\text{-}Scale}$ were enriched from umbilical cord-derived mesenchymal stem cells via differential ultracentrifugation or tangential flow filtration, respectively. Exosomes^{Articial} consisted of dioleoylphosphatidylcholine, cholesterol, dilysocardiolipin, Rab7, Desmoplakin, and AHSG. N = 5, mean ± SEM, two-way ANOVA.

(B and C) *Huntingtin* (*HTT*)-targeting or non-targeting control (*NTC*) siRNAs were infused into the lateral ventricle of mice either alone or in liposomes, Exosome$^{Large\text{-}Scale}$, or Exosomes^{Articial}. *Huntingtin* mRNA were quantified 4 weeks after infusion in striatum (B) and motor cortex (C). N = 5–7, mean ± SD, one-way ANOVA.

to that of Exosomes^{Stressed}. We combined common liposome components (dioleoylphosphatidylcholine and cholesterol) with dilysocardiolipin and palmitoylated Rab7, Desmoplakin, and AHSG in a proteoliposome (Exosome^{Artificial}). Incorporation of three proteins and one lipid to liposomes significantly improved liposome-mediated siRNA transfer to neurons ($p < 0.0001$, two-way ANOVA) (Figure 5A). The efficiency of siRNA-containing artificial exosomes in *Huntingtin* silencing was indistinguishable from that of stressed exosomes (Figure 5A).

To evaluate if siRNA-containing artificial exosomes will support *Huntingtin* silencing *in vivo*, we compared siRNA-containing natural exosomes and artificial exosomes infused into mouse brain. For the *in vivo* study, natural exosomes were produced using a combination of three-dimensional xenofree mesenchymal stem cell culture and tangential flow filtration-based exosome isolation (Exosomes$^{Large\text{-}Scale}$) (Haraszti et al., 2018). This method enabled us to collect a sufficient number of exosomes necessary to power the *in vivo* studies. Natural exosomes (Exosomes$^{Large\text{-}Scale}$) showed an activity indistinguishable from that of Exosomes^{Stressed} and Exosomes^{Artificial} *in vitro* in primary neurons (Figure 5A). When infused to the lateral ventricle of the mouse brain, both Exosomes$^{Large\text{-}Scale}$ and Exosome^{Artifical} loaded with siRNAs induced *Huntingtin* mRNA (Figures 5B and 5C) silencing, whereas control liposomes, non-targeting-control siRNA containing vesicles, and non-formulated siRNA were inactive (Figures 5B and 5C).

DISCUSSION

EVs exhibit specific and efficient intercellular trafficking activity (Valadi et al., 2007; Zomer et al., 2015; Fruhbeis et al., 2013; Monguio-Tortajada et al., 2017; Zhang et al., 2018) and therefore are promising delivery vehicles of various classes of therapeutic proteins and RNAs (Lener et al., 2015; Kramer-Albers, 2017; Kamerkar et al., 2017). However, the mechanisms imparting specific trafficking activity to EVs are unknown. The identification of components necessary and sufficient to make a vesicle behave like an EV would open a new chapter to overcome the delivery challenge of protein- and nucleic acid-based advanced therapeutics.

Serum deprivation of source cells may differentially influence the yield and activity of released EVs. Here we find that serum deprivation of mesenchymal stem cells increases the activity but decreases the yield of exosomes. In contrast, serum deprivation decreases the activity, but does not change the yield of

microvesicles. The concept that serum deprivation may alter the yield of different EV subclasses into different directions has been raised before (Kowal et al., 2016). However, the notion that serum deprivation may increase the activity of one EV subclass but decrease the activity of another EV subclass produced from the same cells has not been described before. This observation indicates that exosome and microvesicle production pathways are differentially regulated in stress conditions.

Exosomes released from stressed cells exhibit a specific enhancement in activity and a specific protein composition. Therefore, stressed exosomes are ideally suited for composition-activity relationship studies. The protein content of EVs from serum-deprived and control cells has been shown to differ (Kowal et al., 2016; Li et al., 2015). The functional 20S proteasome, all subunits of which we find specifically enriched in stressed exosomes, has been detected in EVs before (Bochmann et al., 2014; Kowal et al., 2016) and has been proposed to be of therapeutic value (Lai et al., 2012). We also observe enrichment in desmosomal proteins, ribosomal proteins, histones, and endosomal proteins, all of which have been reported in EVs and are proposed to play a role in an EV release mechanism (Choi et al., 2012; Overmiller et al., 2017; Dozio and Sanchez, 2017; Keerthikumar et al., 2015; Willms et al., 2016; Nemeth et al., 2017; Watson et al., 2012). Several strategies have been successfully applied to modulate the surface of EVs: expressing proteins fused to palmitoylation signals (Lai et al., 2014), transmembrane domains (Lai et al., 2014), or exosomal marker proteins (Yim et al., 2016; Alvarez-Erviti et al., 2011) in producer cells; CLICK chemistry-based conjugation (Smyth et al., 2014); fusing EVs with liposomes (Lee et al., 2015; Sato et al., 2016); and loading cholesterol-conjugated aptamers onto the surface of EVs (Pi et al., 2018). Here we show that three of eight proteins (Desmoplakin, AHSG, and Rab7) enhance vesicle trafficking to neurons. We used chemical palmitoylation to enable protein loading into the vesicle membrane. Different proteins may have different sensitivity to this treatment (i.e., high pH and palmitoylation on lysine residues instead of the naturally occurring cysteine, serine, and threonine residues). Thus the lack of enhancement in liposome neuronal uptake may not indicate a lack of contribution to vesicle trafficking. Further advancement of the technology presented here will require combinatorial optimization of protein loading to membrane as well as lipid-to-protein ratios.

A main finding of this study is the identification of dilysocardiolipin as an essential component of exosomes. We previously have reported on cardiolipin enrichment in exosomes compared with cells and microvesicles (Haraszti et al., 2016). Lysocardiolipins are substrates of a cardiolipin-remodeling enzyme residing in the ER (acyl-coA:lysocardiolipin acyltransferase 1) (Cao et al., 2004). The ER-Golgi secretory pathway (also enriched in stressed exosomes) may overlap with the release of exosomes from the multivesicular body (Friend, 1969; Kolesnikova et al., 2004; Nilsson et al., 2015). Thus dilysocardiolipin may use this overlapping secretory pathway to enter exosomes under stress conditions.

Artificial exosomes constructed from purified lipid and protein components would have several advantages over natural exosomes. First, the manufacture of proteoliposomes is an easily scalable process and may be more cost-effective than manufacturing cell-derived exosomes. Second, the quality control of cell-free artificial exosomes could follow established guidelines from the liposome field, whereas the quality control requirements of natural therapeutic exosomes remain unclear (Lener et al., 2015; Reiner et al., 2017). Third, loading therapeutic cargo (proteins or RNA) into or onto artificial exosomes could be a simple step added to the manufacturing process, whereas efficient loading of therapeutic cargo to natural exosomes is still challenging.

Limitations of the Study

The activity of artificial exosome composition identified here might be limited to neuronal uptake and alteration or optimization of this composition likely is necessary to tune artificial exosomes for delivery to other cell types. The mechanism of action of dilysocardiolipin, Rab7, Desmoplakin, and AHSG may differ in natural and artificial exosomes. The method used here to load proteins onto liposomes (chemical palmitoylation) may have different efficiency for different proteins and may not be suited for all proteins. Loading proteins on the surface of neutral liposomes may alter the surface charge, which in turn may influence cellular uptake. Optimization of the loading method is needed to control the protein-to-lipid ratio in artificial exosomes.

METHODS

All methods can be found in the accompanying Transparent Methods supplemental file.

SUPPLEMENTAL INFORMATION

Supplemental Information can be found online at https://doi.org/10.1016/j.isci.2019.05.029.

ACKNOWLEDGMENTS

This publication is part of the NIH Extracellular RNA Communication Consortium paper package and was supported by the NIH Common Fund's exRNA Communication Program. This work was supported by the NIH UH3 grant TR 000888 05 and the UMass CCTS UL1 TR000161 grant to N.A. and A.K.; NIH grants RO1GM10880304, RO1NS10402201, and S10 OD020012 to A.K.; and the CHDI Foundation (Research Agreement A-6119, JSC A6367) to N.A. M.-C.D. was supported by a Huntington's Disease Society of America Postdoctoral Fellowship and B.M.D.C.G. was supported by a Milton-Safenowitz Fellowship (17-PDF-363) from the Amyotrophic Lateral Sclerosis Association.

AUTHOR CONTRIBUTIONS

Conceptualization, R.A.H., N.A., and A.K.; Methodology & Investigation, R.A.H. (primary neurons, silencing measurements, PNA hybridization assay, confocal microscopy, EV, liposomes and artificial exosome preparations, western blots, nanoparticle tracking analysis, siRNA loading to vesicles, mouse harvest); R.M. (EV preparations), M.-C.D. (EV preparations, cholesterol-siRNA loading to EVs), M.L.D. (proteomics), J.L. (proteomics), S.A.S. (proteomics), H.E.R. (lipidomics), J.M. (lipidomics), N.R.N. (lipidomics), M.A.K. (lipidomics), E.S. (electron microcopy), M.D. (electron microscopy), A.H.C. (mouse surgeries), M.S. (large-scale exosomes), Y.Y.S. (large-scale exosomes), R.W. (large-scale exosomes), Y.W. (large-scale exosomes), J.F.A. (mouse brain harvest), B.M.D.C.G. (mouse brain harvest); Validation, R.A.H. and A.K.; Formal Analysis, R.A.H.; Resources, D.E. (synthesis of siRNAs), M.R.H. (maintenance of oligonucleotide synthesizers and HPLCs); Writing – Original Draft, R.A.H and A.K.; Visualization, R.A.H.; Writing – Review & Editing, N.A.; Supervision, S.A.S., M.A.K., Y.W., M.D., N.A. and A.K.; Project Administration, R.A.H.; Funding Acquisition: N.A. and A.K.

DECLARATION OF INTERESTS

R.A.H., N.A., and A.K. are filing a patent application related to artificial exosomes. Other authors do not have a conflict of interest.

Received: November 6, 2018
Revised: April 4, 2019
Accepted: May 22, 2019
Published: June 28, 2019

REFERENCES

Alterman, J.F., Hall, L.M., Coles, A.H., Hassler, M.R., Didiot, M.C., Chase, K., Abraham, J., Sottosanti, E., Johnson, E., Sapp, E., et al. (2015). Hydrophobically modified siRNAs silence huntingtin mRNA in primary neurons and mouse brain. Mol. Ther. Nucleic Acids *4*, e266.

Alvarez-Erviti, L., Seow, Y., Yin, H., Betts, C., Lakhal, S., and Wood, M.J. (2011). Delivery of siRNA to the mouse brain by systemic injection of targeted exosomes. Nat. Biotechnol. *29*, 341–345.

Aubertin, K., Silva, A.K., Luciani, N., Espinosa, A., Djemat, A., Charue, D., Gallet, F., Blanc-Brude, O., and Wilhelm, C. (2016). Massive release of extracellular vesicles from cancer cells after photodynamic treatment or chemotherapy. Sci. Rep. *6*, 35376.

Bochmann, I., Ebstein, F., Lehmann, A., Wohlschlaeger, J., Sixt, S.U., Kloetzel, P.M., and Dahlmann, B. (2014). T lymphocytes export proteasomes by way of microparticles: a possible mechanism for generation of extracellular proteasomes. J. Cell. Mol. Med. *18*, 59–68.

Cao, J., Liu, Y., Lockwood, J., Burn, P., and Shi, Y. (2004). A novel cardiolipin-remodeling pathway revealed by a gene encoding an endoplasmic reticulum-associated acyl-CoA:lysocardiolipin acyltransferase (ALCAT1) in mouse. J. Biol. Chem. *279*, 31727–31734.

Choi, D.S., Choi, D.Y., Hong, B.S., Jang, S.C., Kim, D.K., Lee, J., Kim, Y.K., Kim, K.P., and Gho, Y.S. (2012). Quantitative proteomics of extracellular vesicles derived from human primary and metastatic colorectal cancer cells. J. Extracell. Vesicles *1*, 18704.

Delva, E., Tucker, D.K., and Kowalczyk, A.P. (2009). The desmosome. Cold Spring Harb. Perspect. Biol. *1*, a002543.

Didiot, M.-C., Hall, L.M., Coles, A.H., Haraszti, R.A., Godinho, B.M.D.C., Chase, K., Sapp, E., Ly, S., Alterman, J.F., Hassler, M.R., et al. (2016). Exosome-mediated delivery of hydrophobically modified siRNA for huntingtin mRNA silencing. Mol. Ther. *24*, 1836–1847.

Dozio, V., and Sanchez, J.C. (2017). Characterisation of extracellular vesicle-subsets derived from brain endothelial cells and analysis of their protein cargo modulation after TNF exposure. J. Extracell. Vesicles *6*, 1302705.

Friend, D.S. (1969). Cytochemical staining of multivesicular body and golgi vesicles. J. Cell Biol. *41*, 269–279.

Fruhbeis, C., Frohlich, D., Kuo, W.P., Amphornrat, J., Thilemann, S., Saab, A.S., Kirchhoff, F., Mobius, W., Goebbels, S., Nave, K.A., et al. (2013). Neurotransmitter-triggered transfer of exosomes mediates oligodendrocyte-neuron communication. PLoS Biol. *11*, e1001604.

Guitart, K., Loers, G., Buck, F., Bork, U., Schachner, M., and Kleene, R. (2016). Improvement of neuronal cell survival by astrocyte-derived exosomes under hypoxic and ischemic conditions depends on prion protein. Glia *64*, 896–910.

Han, Y.D., Bai, Y., Yan, X.L., Ren, J., Zeng, Q., Li, X.D., Pei, X.T., and Han, Y. (2018). Co-transplantation of exosomes derived from hypoxia-preconditioned adipose mesenchymal stem cells promotes neovascularization and graft survival in fat grafting. Biochem. Biophys. Res. Commun. *497*, 305–312.

Haraszti, R.A., Didiot, M.C., Sapp, E., Leszyk, J., Shaffer, S.A., Rockwell, H.E., Gao, F., Narain, N.R., Difiglia, M., Kiebish, M.A., et al. (2016). High-resolution proteomic and lipidomic analysis of exosomes and microvesicles from different cell sources. J. Extracell. Vesicles *5*, 32570.

Haraszti, R.A., Miller, R., Stoppato, M., Sere, Y.Y., Coles, A., Didiot, M.C., Wollacott, R., Sapp, E., Dubuke, M.L., Li, X., et al. (2018). Exosomes produced from 3D cultures of MSCs by tangential flow filtration show higher yield and improved activity. Mol. Ther. *22*, 30456–30458.

Huijbregts, R.P., Topalof, L., and Bankaitis, V.A. (2000). Lipid metabolism and regulation of membrane trafficking. Traffic *1*, 195–202.

Ikonen, E. (2001). Roles of lipid rafts in membrane transport. Curr. Opin. Cell Biol. *13*, 470–477.

Kamerkar, S., Lebleu, V.S., Sugimoto, H., Yang, S., Ruivo, C.F., Melo, S.A., Lee, J.J., and Kalluri, R. (2017). Exosomes facilitate therapeutic targeting of oncogenic KRAS in pancreatic cancer. Nature *546*, 498–503.

Keerthikumar, S., Gangoda, L., Liem, M., Fonseka, P., Atukorala, I., Ozcitti, C., Mechler, A., Adda, C.G., Ang, C.S., and Mathivanan, S. (2015). Proteogenomic analysis reveals exosomes are more oncogenic than ectosomes. Oncotarget *6*, 15375–15396.

King, H.W., Michael, M.Z., and Gleadle, J.M. (2012). Hypoxic enhancement of exosome release by breast cancer cells. BMC Cancer *12*, 421.

Kolesnikova, L., Berghofer, B., Bamberg, S., and Becker, S. (2004). Multivesicular bodies as a platform for formation of the Marburg virus envelope. J. Virol. *78*, 12277–12287.

Kowal, J., Arras, G., Colombo, M., Jouve, M., Morath, J.P., Primdal-Bengtson, B., Dingli, F., Loew, D., Tkach, M., and Thery, C. (2016). Proteomic comparison defines novel markers to characterize heterogeneous populations of extracellular vesicle subtypes. Proc. Natl. Acad. Sci. U S A *113*, E968–E977.

Kramer-Albers, E.M. (2017). Ticket to ride: targeting proteins to exosomes for brain delivery. Mol. Ther. *25*, 1264–1266.

Kummel, D., and Ungermann, C. (2014). Principles of membrane tethering and fusion in endosome and lysosome biogenesis. Curr. Opin. Cell Biol. *29*, 61–66.

Lai, C.P., Kim, E.Y., Badr, C.E., Weissleder, R., Mempel, T.R., Tannous, B.A., and Breakefield, X.O. (2015). Visualization and tracking of tumour extracellular vesicle delivery and RNA translation using multiplexed reporters. Nat. Commun. *6*, 7029.

Lai, C.P., Mardini, O., Ericsson, M., Prabhakar, S., Maguire, C.A., Chen, J.W., Tannous, B.A., and Breakefield, X.O. (2014). Dynamic biodistribution of extracellular vesicles in vivo using a multimodal imaging reporter. ACS Nano *8*, 483–494.

Lai, R.C., Tan, S.S., Teh, B.J., Sze, S.K., Arslan, F., De Kleijn, D.P., Choo, A., and Lim, S.K. (2012). Proteolytic potential of the MSC exosome proteome: implications for an exosome-mediated delivery of therapeutic proteasome. Int. J. Proteomics *2012*, 971907.

Lee, J., Kim, J., Jeong, M., Lee, H., Goh, U., Kim, H., Kim, B., and Park, J.H. (2015). Liposome-based engineering of cells to package hydrophobic compounds in membrane vesicles for tumor penetration. Nano Lett. *31*, 2938–2944.

Lener, T., Gimona, M., Aigner, L., Borger, V., Buzas, E., Camussi, G., Chaput, N., Chatterjee, D., Court, F.A., Del Portillo, H.A., et al. (2015). Applying extracellular vesicles based therapeutics in clinical trials - an ISEV position paper. J. Extracell. Vesicles *4*, 30087.

Li, J., Lee, Y., Johansson, H.J., Mager, I., Vader, P., Nordin, J.Z., Wiklander, O.P., Lehtio, J., Wood, M.J., and Andaloussi, S.E. (2015). Serum-free culture alters the quantity and protein composition of neuroblastoma-derived extracellular vesicles. J. Extracell. Vesicles *4*, 26883.

Mleczko, J., Ortega, F.J., Falcon-Perez, J.M., Wabitsch, M., Fernandez-Real, J.M., and Mora, S. (2018). Extracellular vesicles from hypoxic adipocytes and obese subjects reduce insulin-stimulated glucose uptake. Mol. Nutr. Food Res. *2*, 201700917.

Monguio-Tortajada, M., Roura, S., Galvez-Monton, C., Pujal, J.M., Aran, G., Sanjurjo, L., Franquesa, M., Sarrias, M.R., Bayes-Genis, A., and Borras, F.E. (2017). Nanosized UCMSC-derived extracellular vesicles but not conditioned medium exclusively inhibit the inflammatory response of stimulated T cells: implications for nanomedicine. Theranostics *7*, 270–284.

Nabhan, J.F., Hu, R., Oh, R.S., Cohen, S.N., and Lu, Q. (2012). Formation and release of arrestin domain-containing protein 1-mediated microvesicles (ARMMs) at plasma membrane by recruitment of TSG101 protein. Proc. Natl. Acad. Sci. U S A *109*, 4146–4151.

Nemeth, A., Orgovan, N., Sodar, B.W., Osteikoetxea, X., Paloczi, K., Szabo-Taylor, K.E., Vukman, K.V., Kittel, A., Turiak, L., Wiener, Z., et al. (2017). Antibiotic-induced release of small extracellular vesicles (exosomes) with surface-associated DNA. Sci. Rep. *7*, 8202.

Nilsson, P., Sekiguchi, M., Akagi, T., Izumi, S., Komori, T., Hui, K., Sorgjerd, K., Tanaka, M., Saito, T., Iwata, N., and Saido, T.C. (2015). Autophagy-related protein 7 deficiency in amyloid beta (Abeta) precursor protein transgenic mice decreases Abeta in the multivesicular bodies and induces Abeta accumulation in the Golgi. Am. J. Pathol. *185*, 305–313.

Oskowitz, A., Mcferrin, H., Gutschow, M., Carter, M.L., and Pochampally, R. (2011). Serum-deprived human multipotent mesenchymal stromal cells (MSCs) are highly angiogenic. Stem Cell Res. *6*, 215–225.

Overmiller, A.M., Pierluissi, J.A., Wermuth, P.J., Sauma, S., Martinez-Outschoorn, U., Tuluc, M., Luginbuhl, A., Curry, J., Harshyne, L.A., Wahl, J.K., et al. (2017). Desmoglein 2 modulates extracellular vesicle release from squamous cell carcinoma keratinocytes. FASEB J. *31*, 3412–3424.

Paulmann, M., Arnold, T., Linke, D., Ozdirekcan, S., Kopp, A., Gutsmann, T., Kalbacher, H., Wanke, I., Schuenemann, V.J., Habeck, M., et al. (2012). Structure-activity analysis of the dermcidin-derived peptide DCD-1L, an anionic antimicrobial peptide present in human sweat. J. Biol. Chem. *287*, 8434–8443.

Pi, F., Binzel, D.W., Lee, T.J., Li, Z., Sun, M., Rychahou, P., Li, H., Haque, F., Wang, S., Croce, C.M., et al. (2018). Nanoparticle orientation to control RNA loading and ligand display on extracellular vesicles for cancer regression. Nat. Nanotechnol. *13*, 82–89.

Pope, S.M., and Lasser, C. (2013). Toxoplasma gondii infection of fibroblasts causes the production of exosome-like vesicles containing a unique array of mRNA and miRNA transcripts compared to serum starvation. J. Extracell. Vesicles *2*, 22484.

Reiner, A.T., Witwer, K.W., Van Balkom, B.W.M., De Beer, J., Brodie, C., Corteling, R.L., Gabrielsson, S., Gimona, M., Ibrahim, A.G., De Kleijn, D., et al. (2017). Concise review: developing best-practice models for the therapeutic use of extracellular vesicles. Stem Cells Transl. Med. *6*, 1730–1739.

Sato, Y.T., Umezaki, K., Sawada, S., Mukai, S.A., Sasaki, Y., Harada, N., Shiku, H., and Akiyoshi, K. (2016). Engineering hybrid exosomes by membrane fusion with liposomes. Sci. Rep. *6*, 21933.

Schlame, M., Acehan, D., Berno, B., Xu, Y., Valvo, S., Ren, M., Stokes, D.L., and Epand, R.M. (2012). The physical state of lipid substrates provides transacylation specificity for tafazzin. Nat. Chem. Biol. *8*, 862–869.

Smyth, T., Petrova, K., Payton, N.M., Persaud, I., Redzic, J.S., Graner, M.W., Smith-Jones, P., and Anchordoquy, T.J. (2014). Surface functionalization of exosomes using click chemistry. Bioconjug. Chem. *25*, 1777–1784.

Sun, L., Wang, H.X., Zhu, X.J., Wu, P.H., Chen, W.Q., Zou, P., Li, Q.B., and Chen, Z.C. (2014). Serum deprivation elevates the levels of microvesicles with different size distributions and selectively enriched proteins in human myeloma cells in vitro. Acta Pharmacol. Sin. *35*, 381–393.

Taverna, S., Ghersi, G., Ginestra, A., Rigogliuso, S., Pecorella, S., Alaimo, G., Saladino, F., Dolo, V., Dell'era, P., Pavan, A., et al. (2003). Shedding of membrane vesicles mediates fibroblast growth factor-2 release from cells. J. Biol. Chem. *278*, 51911–51919.

Thery, C., Amigorena, S., Raposo, G., and Clayton, A. (2006). Isolation and characterization of exosomes from cell culture supernatants and biological fluids. Curr. Protoc. Cell Biol. *30*, 3.22.1–3.22.29, Chapter 3, Unit 3 22.

Valadi, H., Ekstrom, K., Bossios, A., Sjostrand, M., Lee, J.J., and Lotvall, J.O. (2007). Exosome-mediated transfer of mRNAs and microRNAs is a novel mechanism of genetic exchange between cells. Nat. Cell Biol. *9*, 654–659.

Watson, K., Koumangoye, R., Thompson, P., Sakwe, A.M., Patel, T., Pratap, S., and Ochieng, J. (2012). Fetuin-A triggers the secretion of a novel set of exosomes in detached tumor cells that mediate their adhesion and spreading. FEBS Lett. *586*, 3458–3463.

Willms, E., Johansson, H.J., Mager, I., Lee, Y., Blomberg, K.E., Sadik, M., Alaarg, A., Smith, C.I., Lehtio, J., El Andaloussi, S., et al. (2016). Cells release subpopulations of exosomes with distinct molecular and biological properties. Sci. Rep. *6*, 22519.

Xie, J.C., Ma, X.Y., Liu, X.H., Yu, J., Zhao, Y.C., Tan, Y., Liu, X.Y., and Zhao, Y.X. (2018). Hypoxia increases amyloid-beta level in exosomes by enhancing the interaction between CD147 and Hook1. Am. J. Transl. Res. *10*, 150–163.

Yang, J., Zhang, X., Chen, X., Wang, L., and Yang, G. (2017). Exosome mediated delivery of miR-124 promotes neurogenesis after ischemia. Mol. Ther. Nucleic Acids *7*, 278–287.

Yim, N., Ryu, S.W., Choi, K., Lee, K.R., Lee, S., Choi, H., Kim, J., Shaker, M.R., Sun, W., Park, J.H., et al. (2016). Exosome engineering for efficient intracellular delivery of soluble proteins using optically reversible protein-protein interaction module. Nat. Commun. *7*, 12277.

Zhang, P., Zhang, L., Qin, Z., Hua, S., Guo, Z., Chu, C., Lin, H., Zhang, Y., Li, W., Zhang, X., et al. (2018). Genetically engineered liposome-like nanovesicles as active targeted transport platform. Adv. Mater. *30*, 27.

Zomer, A., Maynard, C., Verweij, F.J., Kamermans, A., Schafer, R., Beerling, E., Schiffelers, R.M., De Wit, E., Berenguer, J., Ellenbroek, S.I., et al. (2015). In Vivo imaging reveals extracellular vesicle-mediated phenocopying of metastatic behavior. Cell *161*, 1046–1057.

ISCI, Volume *16*

Supplemental Information

Serum Deprivation of Mesenchymal Stem Cells Improves Exosome Activity and Alters Lipid and Protein Composition

Reka Agnes Haraszti, Rachael Miller, Michelle L. Dubuke, Hannah E. Rockwell, Andrew H. Coles, Ellen Sapp, Marie-Cecile Didiot, Dimas Echeverria, Matteo Stoppato, Yves Y. Sere, John Leszyk, Julia F. Alterman, Bruno M.D.C. Godinho, Matthew R. Hassler, Justice McDaniel, Niven R. Narain, Rachel Wollacott, Yang Wang, Scott A. Shaffer, Michael A. Kiebish, Marian DiFiglia, Neil Aronin, and Anastasia Khvorova

Serum deprivation of mesenchymal stem cells improves exosome activity and alters lipid and protein composition

Reka Agnes Haraszti[1*#], Rachael Miller[1,2], Michelle L Dubuke[3], Hannah E Rockwell[4], Andrew H Coles[1], Ellen Sapp[5], Marie-Cecile Didiot[1], Dimas Echeverria[1], Matteo Stoppato[6], Yves Y Sere[6], John Leszyk[3], Julia F Alterman[1], Bruno MDC Godinho[1], Matthew R Hassler[1], Justice McDaniel[4], Niven R Narain[4], Rachel Wollacott[6], Yang Wang[6], Scott A Shaffer[3], Michael A Kiebish[4], Marian DiFiglia[5], Neil Aronin[1,2], Anastasia Khvorova[1,7]

[1]RNA Therapeutics Institute, University of Massachusetts Medical School, Worcester, MA, USA

[2]Department of Medicine, University of Massachusetts Medical School, Worcester, MA, USA

[3]Mass Spectrometry Facility, Biochemistry and Molecular Pharmacology, University of Massachusetts Medical School, Shrewsbury, MA, USA

[4]BERG LLC, Framingham, MA, USA

[5]Mass General Institute for Neurodegenerative Disease, Boston, MA, USA

[6]MassBiologics, Boston, MA

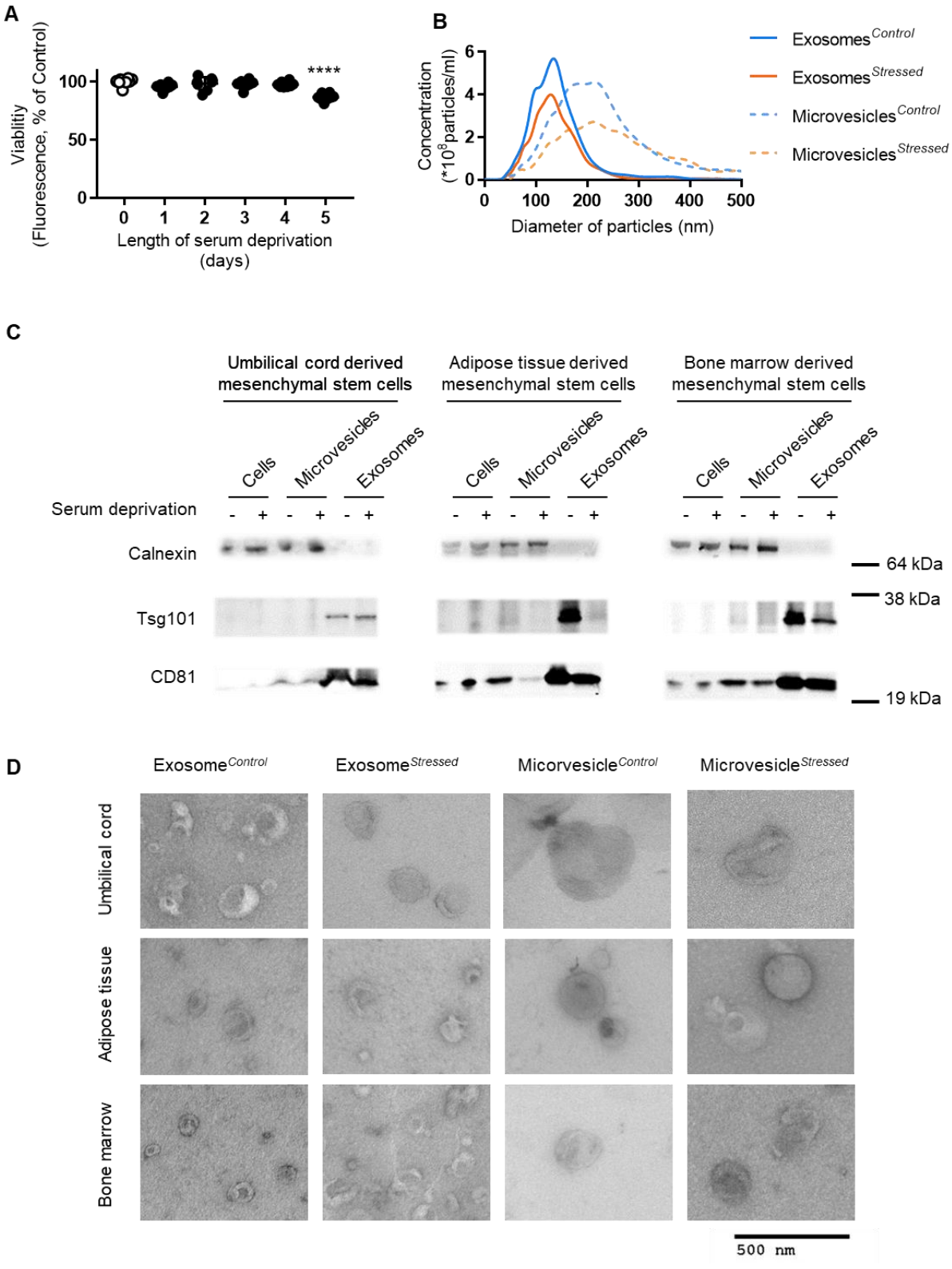
[7]Program in Molecular Medicine, University of Massachusetts Medical School, Worcester, MA, USA

[#]Current address: Universitätklinikum Tübingen, Innere Medizin 2, Otfried-Müller Str. 10., 72076 Tübingen, Germany

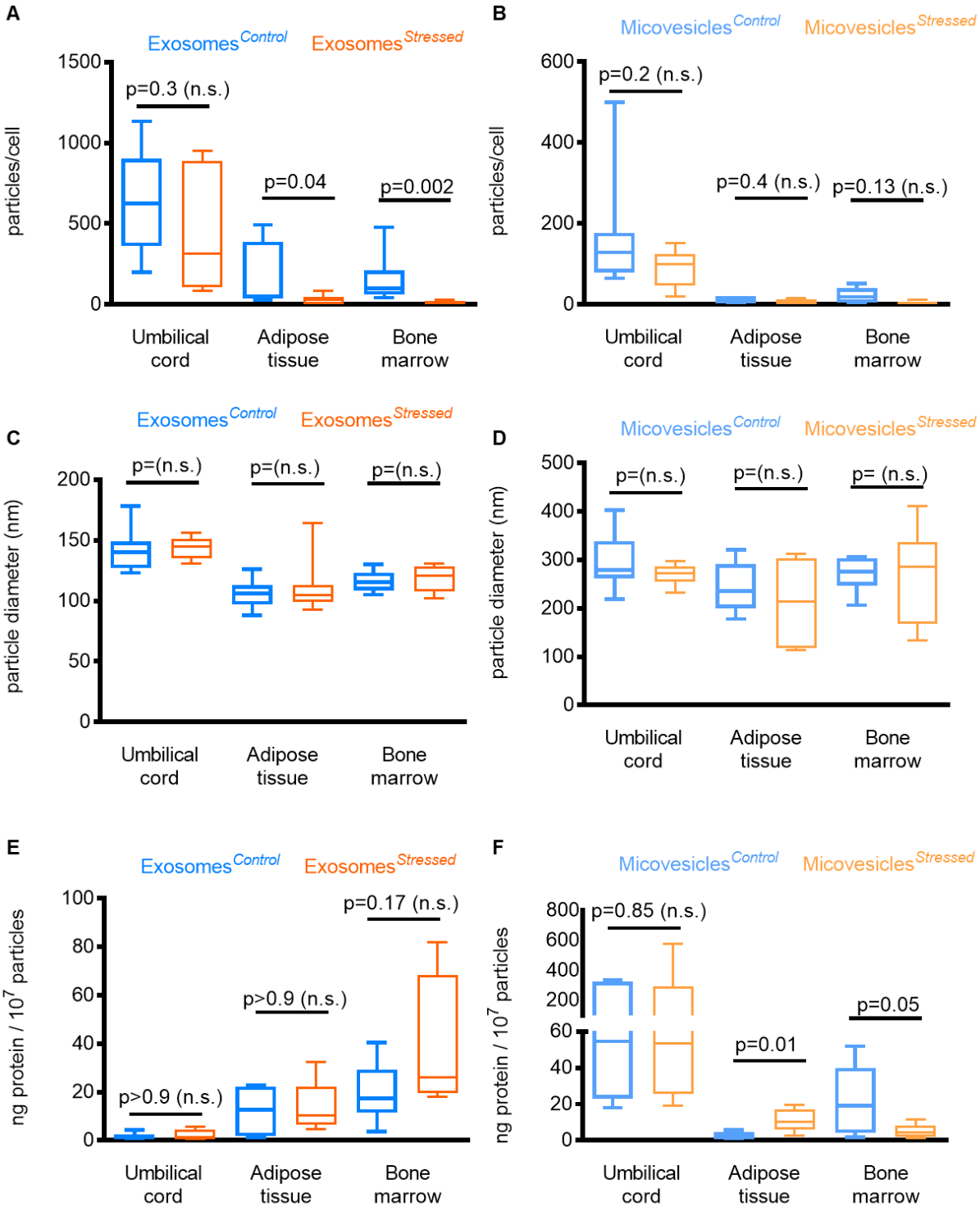
[*]Correspondence should be addressed to:

Reka Agnes Haraszti rharaszti@gmail.com

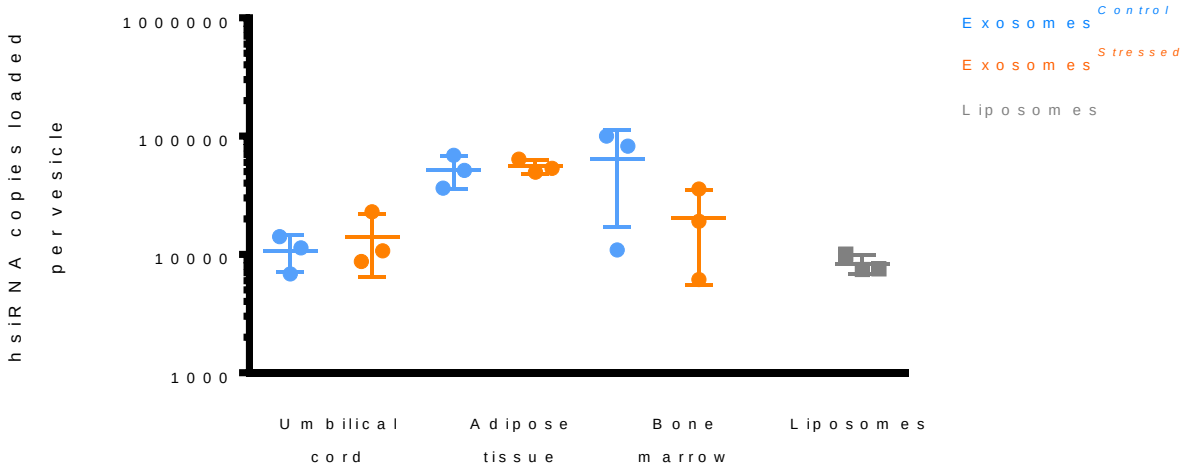
Supplementary Material


A
Viability
(Fluorescence, % of Control)
100
50
0
****
0 1 2 3 4 5
Length of serum deprivation
(days)
B
Concentration
(*10^8 particles/ml)
6
4
2
0
0 100 200 300 400 500
Diameter of particles (nm)
Exosomes Control
Exosomes Stressed
Microvesicles Control
Microvesicles Stressed
C
Umbilical cord derived mesenchymal stem cells
Adipose tissue derived mesenchymal stem cells
Bone marrow derived mesenchymal stem cells
Cells
Microvesicles
Exosomes
Serum deprivation
- + - + - +
Calnexin
Tsg101
CD81
64 kDa
38 kDa
19 kDa
D
Exosome Control
Exosome Stressed
Micorvesicle Control
Microvesicle Stressed
Umbilical cord
Adipose tissue
Bone marrow
500 nm

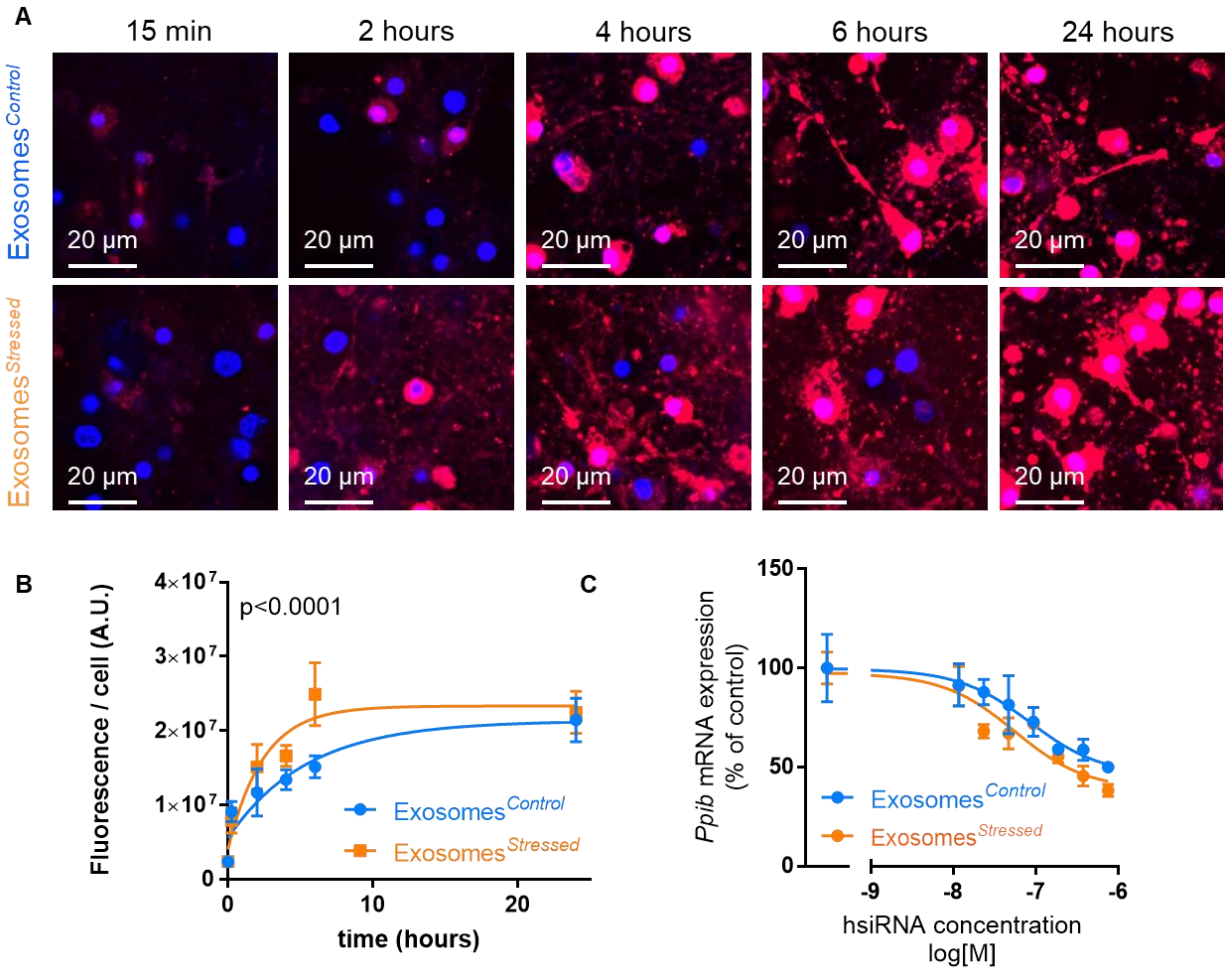
Supplemental Figure 1. Characterization of cell culture conditions and extracellular vesicles. Related to Figures 1, 2 and 4 **A.** Umbilical cord derived mesenchymal stem cells were cultured in either the recommended stem cell medium or in RPMI for differing times. Alamar Blue® was added an incubated at 37℃ for 12 hours, and fluorescence measured at 570 nm excitation, 585 nm emission. Signal is normalized to not serum deprived samples. N = 8, mean ± SD, one-way ANOVA. **B.** Representative size distribution curves of EVs enriched from umbilical cord derived mesenchymal stem cells, N=3, mean, Nanoparticle Tracking Analysis. **C.** Western blots of cells, microvesicles and exosomes derived under control or serum deprived conditions from umbilical cord, adipose tissue or bone marrow derived mesenchymal stem cells. Negative marker: calnexin. Positive markers: Tsg101, CD81. **D.** Representative transmission electron microscopy images of EVs derived under control or serum deprived conditions from umbilical cord, adipose tissue or bone marrow derived mesenchymal stem cells.


A
Exosomes Control
Exosomes Stressed
particles/cell
1500
1000
500
0
p=0.3 (n.s.)
p=0.04
p=0.002
Umbilical cord
Adipose tissue
Bone marrow
B
Micovesicles Control
Micovesicles Stressed
particles/cell
600
400
200
0
p=0.2 (n.s.)
p=0.4 (n.s.)
p=0.13 (n.s.)
Umbilical cord
Adipose tissue
Bone marrow
C
Exosomes Control
Exosomes Stressed
particle diameter (nm)
200
150
100
50
0
p=(n.s.)
p=(n.s.)
p=(n.s.)
Umbilical cord
Adipose tissue
Bone marrow
D
Micovesicles Control
Micovesicles Stressed
particle diameter (nm)
500
400
300
200
100
0
p=(n.s.)
p=(n.s.)
p= (n.s.)
Umbilical cord
Adipose tissue
Bone marrow
E
Exosomes Control
Exosomes Stressed
ng protein / 10^7 particles
100
80
60
40
20
0
p=0.17 (n.s.)
p>0.9 (n.s.)
p>0.9 (n.s.)
Umbilical cord
Adipose tissue
Bone marrow
F
Micovesicles Control
Micovesicles Stressed
ng protein / 10^7 particles
800
600
400
200
60
40
20
0
p=0.85 (n.s.)
p=0.01
p=0.05
Umbilical cord
Adipose tissue
Bone marrow

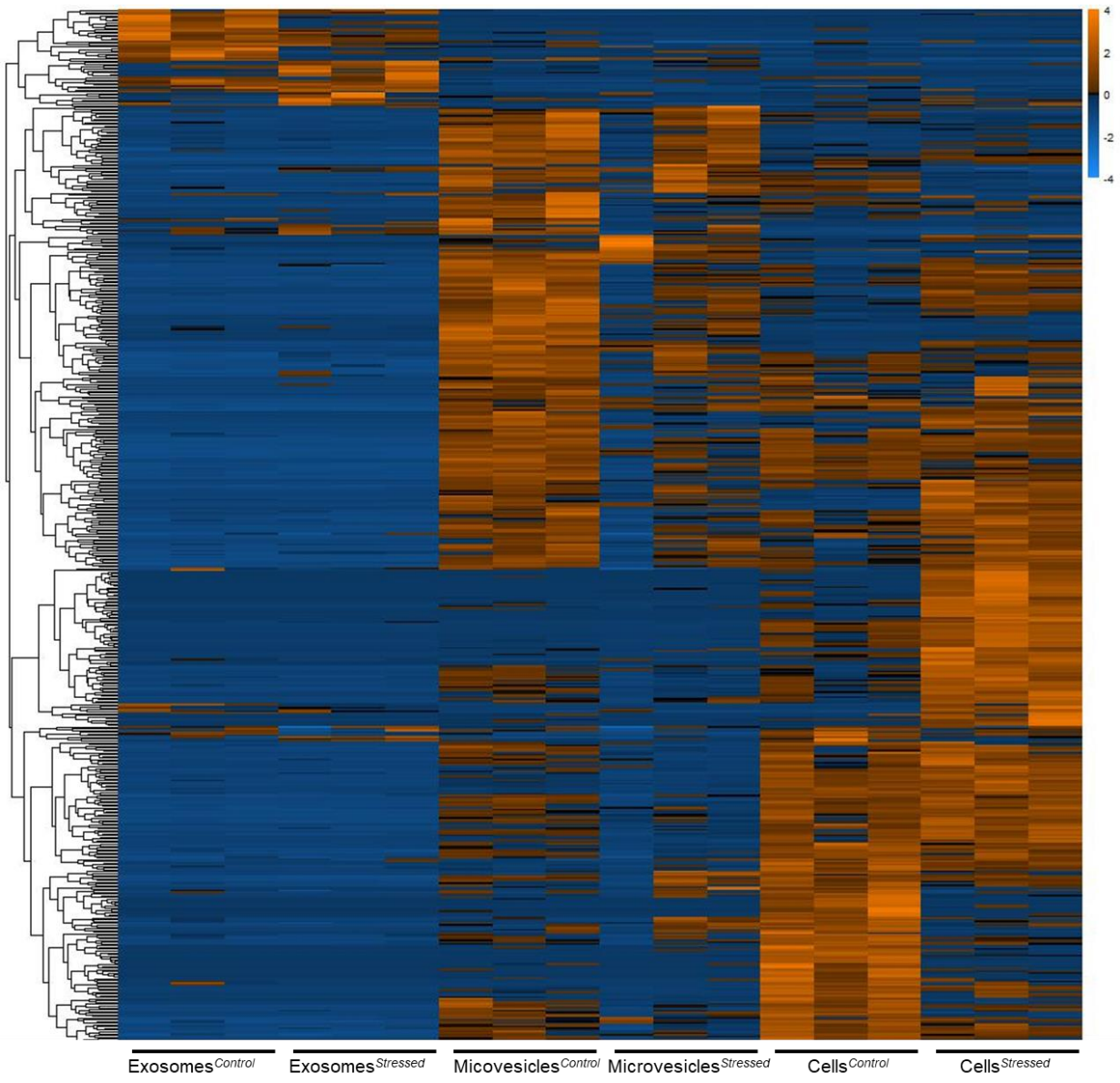
Supplemental Figure 2. Serum deprivation of source cells alters yield and protein-to-vesicle ratio of extracellular vesicles. Related to Figures 1,2, and 4. Extracellular vesicles (EVs) were purified from umbilical cord, adipose tissue or bone marrow derived mesenchymal stem cells *via* differential ultracentrifugation. Cells were cultured under control condition or serum deprived for 24 hours. N=7, lines represent mean, boxes represent 25-75 percentile range and whiskers represent the minimum and maximum value in each group. n.s. = non-significant ($p>0.05$), Mann-Whitney test **A.** Yield, **C.** Size, and **E.** Protein-to-particle ratio of exosomes enriched from conditioned media of control or stressed mesenchymal stem cells *via* differential ultracentrifugation (100 000 g fraction). **B.** Yield, **D.** Size, and **F.** Protein-to-particle ratio of microvesicles enriched from conditioned media of control or stressed mesenchymal stem cells *via* differential ultracentrifugation (10 000 g fraction).



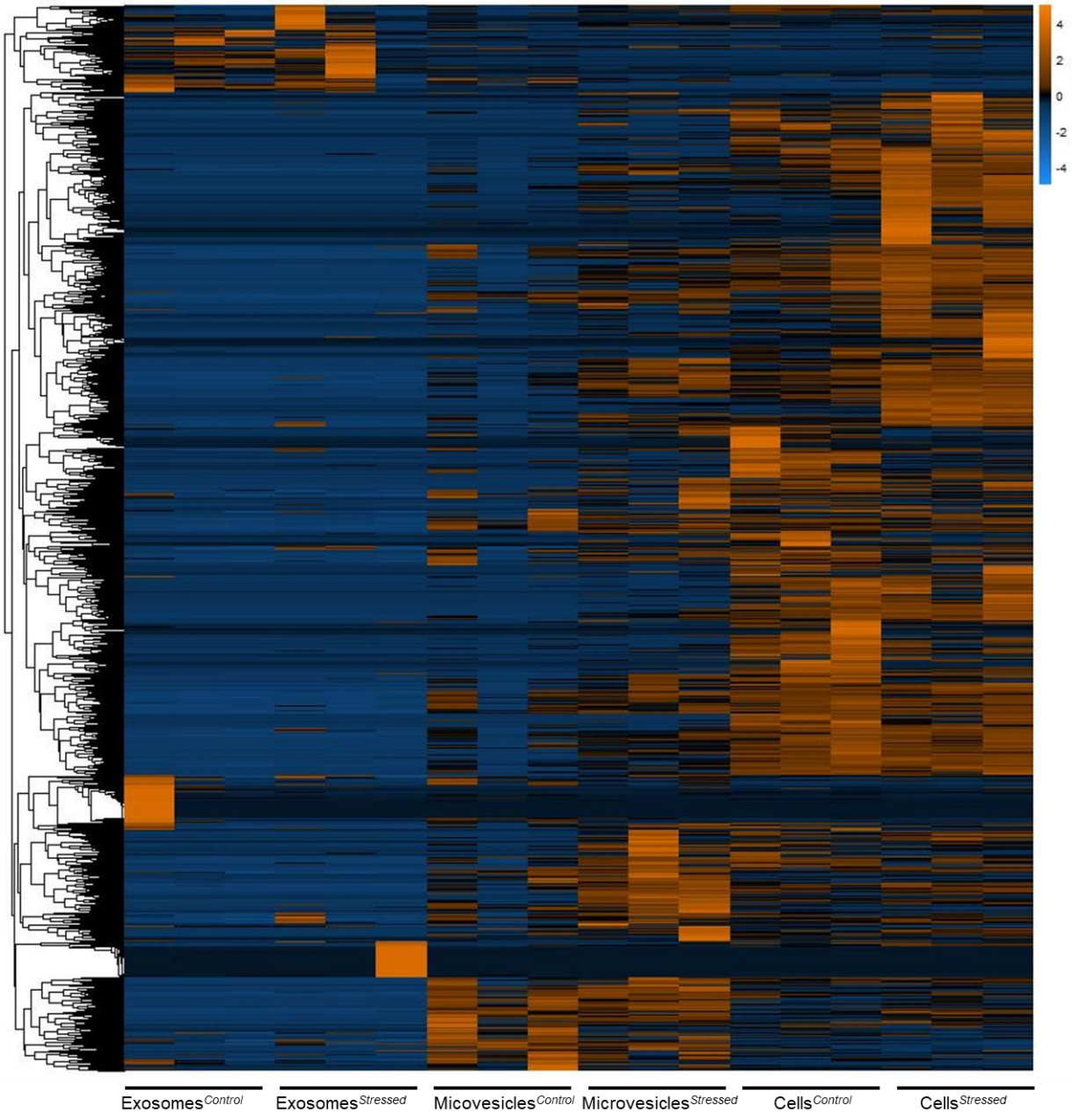
Supplemental Figure 3. Serum deprivation of source cells does not alter the siRNA loading capacity of extracellular vesicles. Related to Figure 1. Exosomes isolated from 3000 cm^2 mesenchymal stem cell culture were quantified and subsequently co-incubated with 150 pmol cholesterol-conjugated fluorescent siRNAs at 37°C for one hour. Then the exosome-siRNA mixture was centrifuged at 100 000 g for 90 min supernatant containing unloaded siRNA removed. Pellet was taken up in PBS for quantification of loading. Percent of loaded siRNA was calculated as follows: pellet / (pellet + supernatant). To estimate siRNA copy number per exosome, the following formula was used: (percent of loaded siRNA) * (amount of siRNA initially mixed in with EVs (mol)) * (Avogadro number) / (number of EVs initially mixed in). Liposomes (grey) had similar siRNA loading capacity to that of natural exosomes. N=3, mean ±SD



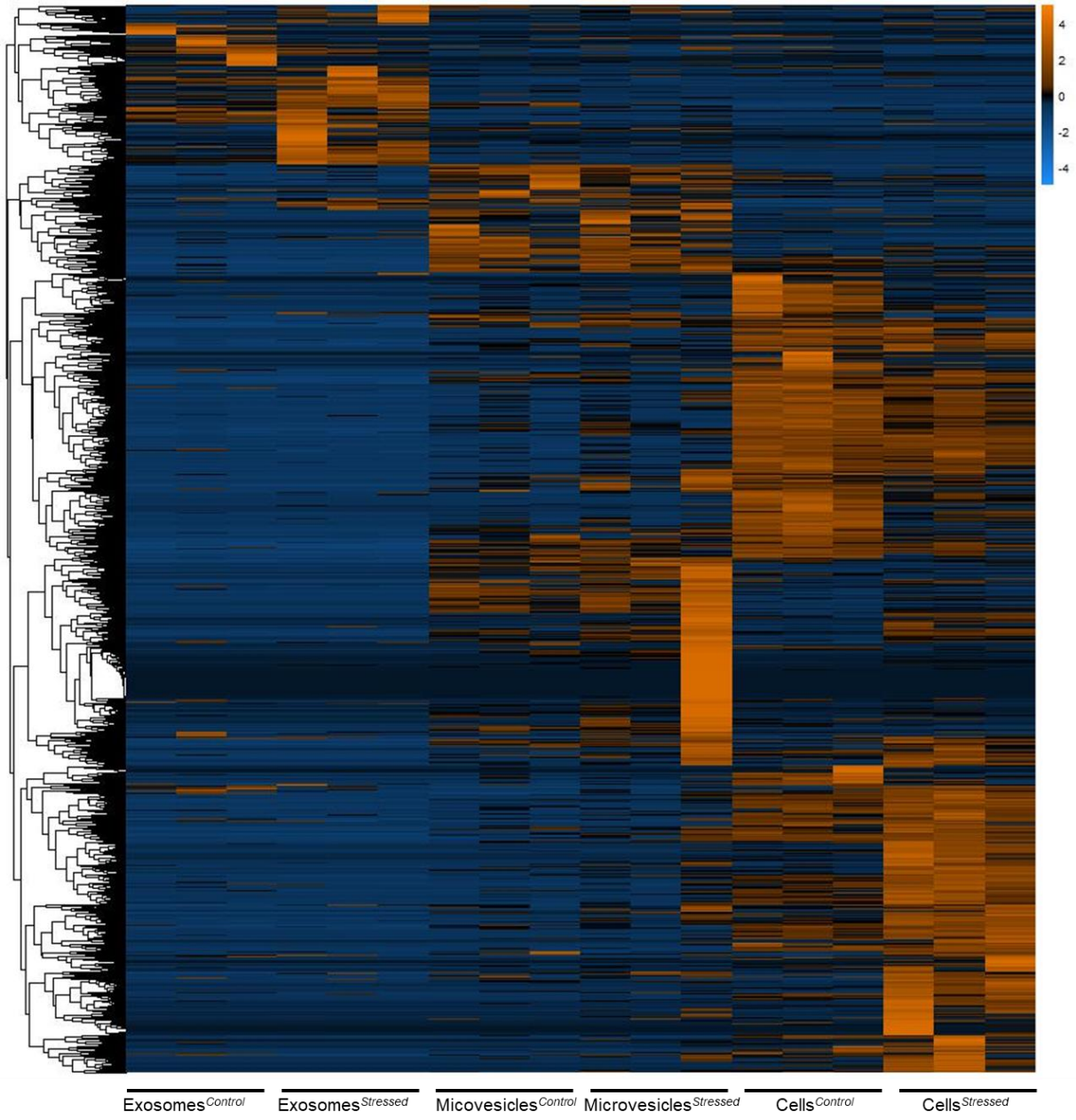
Supplemental Figure 4. Neuronal uptakes of control and stressed exosomes. Related to Figure 1. Primary cortical neurons were cultures on glass bottom plates and treated with fluorescent siRNA containing Exosomes^{Control} or Exosomes^{Stressed}. **A.** Fluorescence was monitored over time using confocal microscopy. Red: siRNA, Blue: nuclei. **B.** Red signal in images were quantified in ImageJ software, N= 39-50 cells per timepoint and kinetic curves compared using two-way ANOVA. **C.** Primary neurons were treated with fluorescent siRNA-containing exosomes derived from control or stressed (serum deprived) cells. After 7 days of incubation, target mRNA levels (*Ppib*) were quantified in neurons. mRNA levels were normalized to housekeeping gene and to untreated control. N=3, mean ± SEM.



Supplemental Figure 5. Proteomics analysis of umbilical cord derived mesenchymal cells and EVs under control or stressed conditions. Related to Figure 2. Label-free quantification was carried out using the intensity-base absolute quantification method. Heatmap was then generated in R, using "pheatmap" package, hierarchical clustering of rows, scaling method: "row".

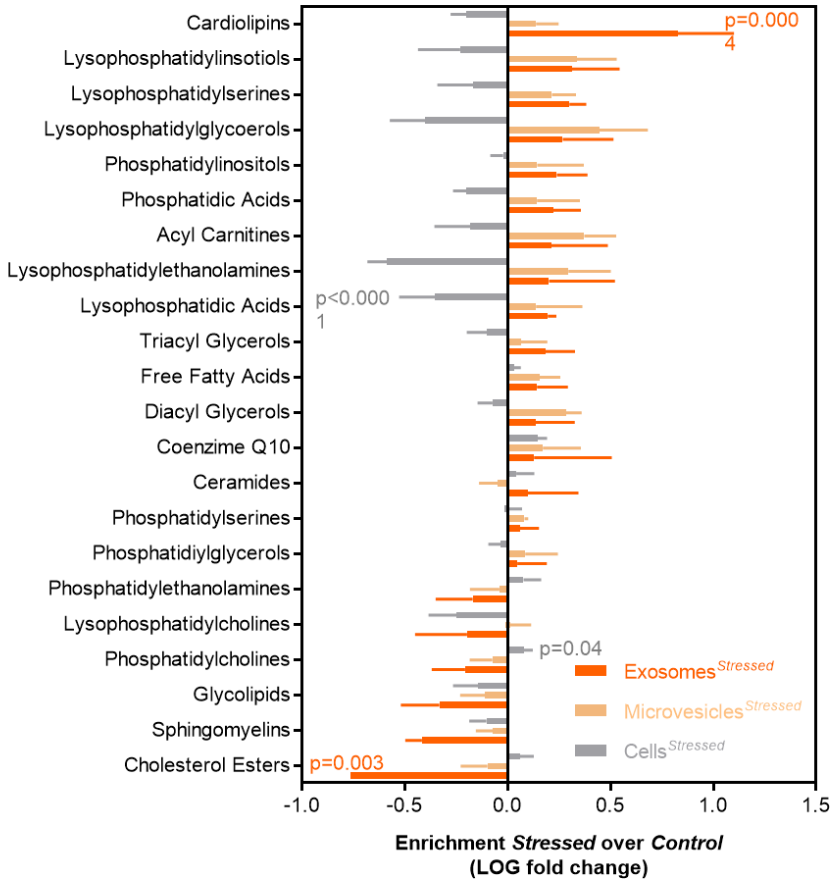


Supplemental Figure 6. Proteomics analysis of adipose tissue derived mesenchymal cells and EVs under control or stressed conditions. Related to Figure 2. Label-free quantification was carried out using the intensity-base absolute quantification method. Heatmap was then generated in R, using "pheatmap" package, hierarchical clustering of rows, scaling method: "row".

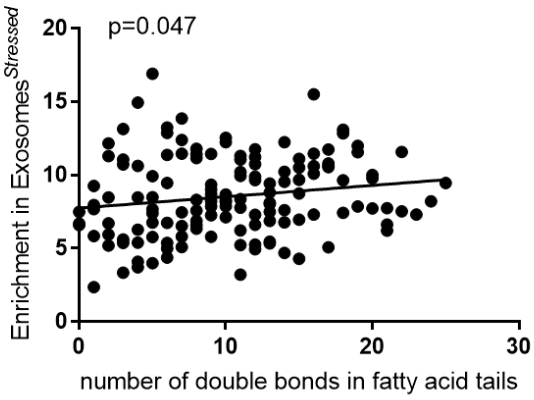


Supplemental Figure 7. Proteomics analysis of bone marrow derived mesenchymal cells and EVs under control or stressed conditions. Related to Figure 2. Label-free quantification was carried out using the intensity-base absolute quantification method. Heatmap was then generated in R, using "pheatmap" package, hierarchical clustering of rows, scaling method: "row".

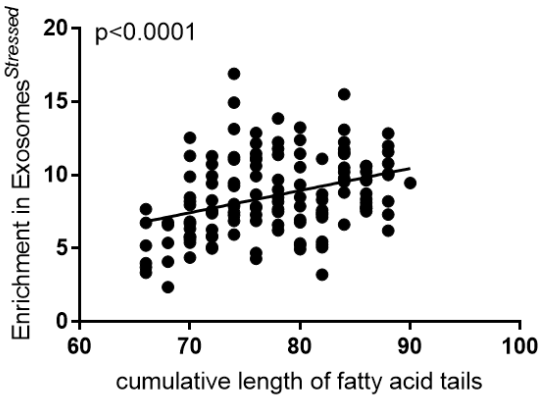
A


Cardiolipins
Lysophosphatidylinsotiols
Lysophosphatidylserines
Lysophosphatidylglycoerols
Phosphatidylinositols
Phosphatidic Acids
Acyl Carnitines
Lysophosphatidylethanolamines
Lysophosphatidic Acids
Triacyl Glycerols
Free Fatty Acids
Diacyl Glycerols
Coenzime Q10
Ceramides
Phosphatidylserines
Phosphatidiylglycerols
Phosphatidylethanolamines
Lysophosphatidylcholines
Phosphatidylcholines
Glycolipids
Sphingomyelins
Cholesterol Esters
p=0.0004
p<0.0001
p=0.04
p=0.003
Exosomes Stressed
Microvesicles Stressed
Cells Stressed
-1.0
-0.5
0.0
0.5
1.0
1.5
Enrichment Stressed over Control
(LOG fold change)

B


p=0.047
Enrichment in Exosomes Stressed
0
5
10
15
20
0
10
20
30
number of double bonds in fatty acid tails

C


p<0.0001
Enrichment in Exosomes Stressed
0
5
10
15
20
60
70
80
90
100
cumulative length of fatty acid tails

Supplemental Figure 8. Serum deprivation of umbilical cord derived mesenchymal stem cells alters lipid composition of exosomes. Related to Figure 4. Umbilical cord derived mesenchymal stem cells and EVs from control or stress conditions (serum deprivation) underwent MS/MS^{ALL} lipidomics analysis. **A.** Bar graph shows of lipid classes in stressed conditions *versus* control conditions. $Exosomes^{Stressed}$ *versus* $Exosomes^{Control}$ (dark orange), $Microvesicles^{Stressed}$ *versus* $Microvesicles^{Control}$ (light orange), and $Cells^{Stressed}$ *versus* $Cells^{Control}$ (grey). N = 2-5, mean ± SD, two-way ANOVA. **B.** Correlation of enrichment in $Exosomes^{Stressed}$ *versus* $Exosomes^{Control}$ with the cumulative number of double bonds in the fatty acid tails of a cardiolipin species (N = 149). Each dot represents a cardiolipin species. **C.** Correlation of enrichment in $Exosomes^{Stressed}$ *versus* $Exosomes^{Control}$ with the cumulative length of the fatty acid tails of a cardiolipin species (N = 149). Each dot represents a cardiolipin species.

Transparent Methods

Oligonucleotides

siRNAs were conjugated to cholesterol at the 3′end of the passenger strand *via* a TEG linker and were fully chemically modified with 5′-vinylphosphonate on the guide strand and an alternating pattern of 2′-*O*-methyls and 2′- fluoros on both strands[1]. PNA oligos were purchased from PNA Bio (*PNA Bio*, *Newbury Park*, *CA*). siRNA and PNA sequences and chemical modification patterns used in this study are described in Supplementary Table 1**.**

siRNAs used in this manuscript were synthesized in house using standard phosphoramidite chemistry and an Expedite ABI DNA/RNA Synthesizer. Each synthesis was done at a 10-µmole scale using a cholesterol-conjugated CPG for the sense strand and a Unylinker® terminus (*ChemGenes, Wilmington, MA*) for the antisense strand. Phosphoramidites were prepared as 0.15 M solutions for 2´-*O*-methyl (*ChemGenes, Wilmington, MA*) and 0.13 M for 2´-fluoro (*BioAutomation, Irving, Texas*) in anhydrous acetonitrile. 0.25 M5-(Benzylthio)-1H-tetrazole in anhydrous acetonitrile was used as coupling activator. Detritylations were performed using 3% dichloroacetic acid in dichloromethane for 80 seconds and capping was performed mixing 16% N-methylimidazole in tetrehydrofurane (CAP A) and 80:10:10 (v/v/v) tetrhydrofurane:acetic anhydride:2,6-lutidine (CAP B) for 15 s. Sulfurizations were carried out with 0.1 M 3-((Dimethylamino-methylidene)amino)-3H-1,2,4-dithiazole-3-thione in (9:1) pyridine:acetonitrile for 3 minutes. Oxidation was performed using 0.02 M iodine in THF:pyridine:water (70:20:10, v/v/v) for 80 s. Phosphoramidite coupling times were 250 s for all amidites. Vinylphosphonate phosphoramidite was dissolved in 40% dichloromethane in acetonitrile to a final concentration of 0.15 sM. For the coupling step, a

4-fold excess of phosphoramidite was loaded on the solid support, and phosphoramidite condensation was carried out for 20 min. A solution of 3% trichloroacetic acid in dichloromethane was used to remove the dimethoxytrityl group from the 5' hydroxyl group of the nucleotide. A solution of 0.25 M 5-(Ethylthio)-1H-tetrazole in anhydrous acetonitrile was used as an activator for the coupling step. Phosphorothioate linkages were introduced using a 0.05 M solution of 3-((dimethylaminomethylene)amino)-3H-1,2,4-dithiazole-5-thione in pyridine:CH3CN (1:1) and a 5 min contact. Solid support was washed with anhydrous acetonitrile then anhydrous dichloromethane and flushed with argon.

Cell culture

Umbilical cord, Wharton's jelly-derived mesenchymal stem cells (PCS -500-010, *ATCC, Manassas, VA*), adipose tissue derived mesenchymal stem cells (PCS-500-011, *ATCC, Manassas, VA*), and bone marrow derived mesenchymal stem cells (Poetics™, PT-2501, *Lonza, Basel, Switzerland*) were cultured in appropriate stem cell medium (PCS-500-030, *ATCC, Manassas, VA,* for umbilical cord and adipose tissue derived cells, and MSCGM™, PT-3238, , *Lonza, Basel, Switzerland* for bone marrow derived cells) in the presence of supplements containing serum and growth factors (PCS-500-040, *ATCC, Manassas, VA* and PT-3001, *Lonza, Basel, Switzerland*) at 37°C, 5% CO_2. Medium was changed every three days, and cells expanded until passage 12, to reach a total of 3000 cm^2 surface in T500 triple flasks. For serum deprivation medium was changed to RPMI (GIBCO™ RPMI 1640, *Thermo Fisher Scientific*) with no FBS or other supplements added for 24 hours.

EV isolation and characterization

Medium on umbilical cord-derived mesenchymal stem cells was changed to EV-depleted medium (centrifuged at 100 000 g for at least 17 hours) or to RPMI (GIBCO™ RPMI 1640, *Thermo Fisher Scientific*) with no FBS or other supplements added and incubated for 24 hours. EVs were then isolated from this conditioned medium *via* differential ultracentrifugation[2,3]. Cell debris was pelleted at 300 g (10 min). Larger EVs or microvesicles were pelleted at 10 000 g (30 min), then supernatant filtered through a 0.2 µm membrane (Nalgene® aPES, *Thermo Fisher Scientific, Waltham, MA*) and small EVs or exosomes pelleted at 100 000 g (90 min) using 70 ml polycarbonate bottles (*Beckman Coulter, Brea, CA;* #355622) and Type 45 Ti rotor (*Beckman Coulter, Brea, CA;* #339160). Microvesicles and exosome pellets were then washed once in 1 ml sterile PBS and centrifuged again for 30 min at 10 000 g or for 90 min at 100 000 g, respectively.

For Western blot analyses, EVs or cell pellets were suspended in RIPA buffer (Pierce® 899000, *Thermo Fisher Scientific, Waltham, MA*) containing PMSF (36978, *Thermo Fisher Scientific*) and protease inhibitor cocktail (cOmplete Mini, 11836153001, *Roche, Indianapolis, IN*), and samples were sonicated for 15 min. Insoluble material was pelleted by centrifugation for 15 minutes at 10 000 g, 4°C. Proteins (50µg) were loaded onto NuPAGE 4–12% Bis-Tris gels (*Thermo Fisher Scientific, Waltham, MA*). After transfer to PVDF (*BioRad, Hercules, CA*), membranes were incubated with antibodies, washed, and images captured using an Odyssey® system (*Li-Cor, Bad Homburg, Germany*) according to manufacturer's instructions. Primary antibodies used were Calnexin (C5C9, *Cell Signaling, Danvers, MA*), Tsg101 (4A10, *Abcam, Cambridge, MA*), CD81 (B11, *Santa Cruz Biotechnology, Dallas, TX*).

Concentration and size distribution of exosomes were measured by Nanoparticle Tracking Analysis (NanoSight NS300, *Malvern*). Briefly, samples were diluted in PBS 1:100 – 1:1000, manually injected into the instrument and videos acquired at ambient temperature at

camera level 9 for 1 minute per sample, N=3. EVs were then frozen at -80°C in 0.1M sucrose and protease inhibitor cocktail (*Sigma-Aldrich, St. Louis, MO, #P8340*) until further use. Transmission Electron Microscopy of EVs was conducted at Mass General Hospital using a JEOL 1100 transmission electron microscope (*JEOL, Peabody, MA*) at 60 kV and AMT digital camera (*Advanced Microscopy Techniques, Woburn, MA*). Samples and grids for were prepared at room temperature. An equal volume of 4% paraformaldehyde was added to the exosome samples and incubated for 2 hours. Aliquots of exosomes (3 µl) were dropped onto grids and incubated in 2% paraformaldehyde for 20 minutes. The grids were transferred to a wax strip and washed with 100 µl PBS. The grids were then incubated in 50 mmol/l glycine/PBS for 5 minutes and blocked in 5% bovine serum albumin/PBS for 10 minutes. The grids were then washed twice in PBS and incubated in 1% glutaraldehyde for 5 minutes. Following eight washes with water of 2 minutes each, the grids were incubated in uranyl oxalate for 5 minutes, and then in a 9:1 solution of 1% methyl cellulose and 4% uranyl acetate for 10 minutes on ice. Excess liquid was removed with a filter paper and the grids were air-dried
for 5–10 minutes.

For large-scale exosome production[4], umbilical cord-derived mesenchymal stem cells were cultured in spinner flasks (250-ml) containing on Star-Plus Microcarriers (SoloHill®, *Pall Life Sciences, Port Washington, NY*) in serum-free and xenofree StemPro® medium was added (A1067501, *Life Technologies, Carlsbad,CA*). Conditioned medium was collected after 48 hours. Collection was performed four times; conditioned medium was stored at 4℃ and subsequently pooled together (final volume 1L). The conditioned medium was filtered through a 0.2 µm polyethersulfone (PES) membrane. Conditioned medium was then subjected to ultrafiltration (9-

fold concentration) in a tangential flow filtration system using a 500 kDa cutoff TFF cartridge (MidiKros® mPES 115 cm^2, D02-E500-05-S*, Spectrum Labs, Rancho Dominguez, CA*) and buffer exchanged with 6x volume of PBS. The exosomes were 0.2 µm filtered (PES membrane) and stored in 0.1M sucrose at -80℃ until further use.

siRNA loading to EVs and liposomes

EVs isolated from 3000 cm^2 mesenchymal stem cell culture were quantified (see above) and subsequently co-incubated with 150 pmol cholesterol-conjugated fluorescent (Cy3-conjugated) siRNAs at 37°C for one hour in 500 µl PBS (loading mixture). Then the EV-siRNA mixture was centrifuged at 100 000 g for 90 min (for exosomes) or at 10 000 g for 30 min (for microvesicles) and supernatant containing unloaded siRNA removed (supernatant). Pellet was taken up in 50 µl PBS for quantification of loading. Fluorescence was assessed at 550 nm excitation, 570 nm emission on TECAN instrument. Percent of loaded siRNA was calculated as follows: pellet / (pellet + supernatant). To estimate siRNA copy number per EV, the following formula was used: (percent of loaded siRNA) * (amount of siRNA initially mixed in with EVs (mol)) * (Avogadro number) / (number of EVs initially mixed in).

Following quantification of loading loaded exosomes were further diluted in 250 µl Neural Q medium for treatment of primary neurons and 50 µl PBS per mouse for mouse infusions. Liposomes were loaded identical to exosomes, e.g. post-synthesis. mRNA silencing experiments were normalized to the amount of siRNA loaded in each individual EV sample.

Proteomics

Protein extraction followed the same protocol as for Western blotting. Total protein (50µg) was applied to an SDS-PAGE gel. Once the entire protein sample entered the stacking gel, electrophoresis was stopped, and the portion of gel containing proteins was excised and stained with Coomassie brilliant blue. The fixed gel fragments were processed by University of Massachusetts Medical School Mass Spectrometry Core[5]. Proteins underwent in-gel trypsin digestion for 21 hours at 37°C, extracted from gels using 80:20 solution of acetonitrile: 1% formic acid, dried in a Speed Vac and pellets redissolved in 5% acetonitrile in 0.1% trifluroacetic acid. Digested protein aliquots were injected into a custom packed 2cm x 100µm C_{18} Magic 5µm particle trap column and samples sprayed on a Waters Nano Acquity UPLC system. Data dependent acquisitions were performed on a Q Exactive mass spectrometer (*Thermo Fisher Scientific, Waltham, MA*), full MS scans from 300-1750 m/z were acquired at a resolution of 70,000 followed by 10 MS/MS scans acquired under HCD fragmentation at a resolution of 17,500 and an isolation width of 1.6 Da. Raw data files were processed with Proteome Discoverer (version 1.4) before using Mascot Server (version 2.5) to search against the Uniprot_Human protein database. Applied search parameters were fully tryptic with 2 missed cleavages, parent mass tolerances of 10 ppm and fragment mass tolerances of 0.05 Da. Search results were loaded into the Scaffold Viewer (Proteome Software, Inc.) to quantify and analyze peptides.

Lipidomics

Frozen EV pellets were transferred to BERG LLC (Framingham, MA) on dry ice for lipid composition analysis as described before[6]. Briefly, aliquots of each sample were combined with a cocktail of deuterium-labeled and odd chain fatty acid standards. Standards were chosen that represent each lipid class and were at designated concentrations expected to provide the most

accurate quantitation of each lipid species. Lipids were extracted with 4 mL of a 1:1 (v/v) solution of chloroform:methanol[7], using an automated custom sequence routine on a Star Hamilton Robotics system (Hamilton, Reno, NV). Lipid extracts were dried under nitrogen and pellets were dissolved in 300 µl of a 1:1 (v/v) solution of chloroform:methanol per mg of protein. Samples were flushed with nitrogen and stored at -20°C. For MS analysis, samples were diluted 50-fold in 3:3:3:1 (v/v/v/v) isopropanol:methanol:acetonitrile:water containing 2mM ammonium acetate to enhance ionization efficiency in positive and negative modes. Electrospray ionization-MS was performed on a SCIEX TripleTOF® 5600^{+} (SCIEX) coupled to a customized direct injection loop system on an Ekspert microLC200 system. 50µl of sample was injected at a flowrate of 6µl/min. Lipids were analyzed using a customized data independent analysis strategy on the TripleTOF® 5600^{+} allowing for MS/MS^{ALL} high resolution and high mass accuracy analysis[8]. Lipids were quantified using an in-house library on MultiQuant™ software.

Liposome and artificial exosome preparation

Conventional liposomes: Dioleoyl-phosphatidylcholine (DOPC) (*#850375, Avanti Polar Lipids, Alabaster, AL*) and cholesterol (, *#700000, Avanti Polar Lipids, Alabaster, AL*) were diluted in chloroform at a concentration of 50 mg/ml. 35 µl of DOPC and 15 µl of cholesterol was transferred into a glass vial and chloroform was evaporated under argon flow. The resulting lipid film was rehydrated in 500 µl of PBS (*#21-031-CV, Dulbecco's Phosphate Buffered Saline, Corning, Manassas, VA*), sonicated for 15 minutes in water bath (*#BB5510, Branson ultrasonic cleaner 40 kHz, Cleanosonic, Richmond VA*), and the extruded using Mini-Extruder (*#610000,Avanti Polar Lipids, Alabaster, AL*) through a 50 nm pore sized polycarbonate membrane (*#WHA800308, Whatman® Nucleopore™, MilliporeSigma, St Louis, MO*). Liposomes were always used fresh, never frozen.

Cardiolipin containing liposomes: Cariolipin (#840012, *Avanti Polar Lipids, Alabaster, AL),* monolysocardiolipin (#850081, *Avanti Polar Lipids, Alabaster, AL)* and dilysocardiolipin

(#850082, *Avanti Polar Lipids, Alabaster, AL)* were diluted in chloroform at a concentration of 10 mg/m. 20 µl DOPC, 15 µl cholesterol and 75 µl cardiolipin, or monolyoscariolipin or dilysocardiolipin were mixed together and liposomes prepared as for conventional liposomes. This composition is equivalent to 40:30:30 w/w ratio of DOPC:cholesterol: cardiolipin/monolysocardiolipins/dilysocardiolipin.

Proteoliposomes; Purified proteins were purchased as follows: Rab7 (TP301776, *OriGene, Rockville, MD*), AHSG (TP723089, *OriGene, Rockville, MD*), Rab5 (TP303873, *OriGene, Rockville, MD*), Desmocollin (TP322207, *OriGene, Rockville, MD*), ARRDC1 (TP307160, *OriGene, Rockville, MD*), Dermcidin (TP309352, *OriGene, Rockville, MD*), Histone 1 (TP301249, *OriGene, Rockville, MD*), Desmoplakin (RPU51172, *Biomatik, Wilmington, DE*). Lyophilized proteins (AHSG and Desmoplakin) were dissolved in 0.1M sodium bicarbonate in PBS (pH=8.5). Proteins delivered in Tris-based buffers (Rab5, Desmocollin, ARRDC1, Dermcidin and Histone 1) underwent buffer exchange using 2K MWCO cutoff membrane dialysis devices (Slide-A-Lyzer™ Mini, #69553, *Thermo Fisher Scientific, Waltham, MA)* 10 µl of sample against 1 l of 0.1M sodium bicarbonate in PBS (pH=8.5) at 4℃ overnight. Palmitic acid N-hydroxysuccinimide ester (palmitoyl-NHS) (P1162, *Sigma-Aldrich, St. Louis, MO)* was added to protein samples in a 1:1 molar ratio to the amount of lysines (lysine frequency was estimated to be 7%) and incubated on a rotating wheel at 4℃ overnight. Palmitoyl-NHS – protein reaction mixture (equivalent of 1 µg protein) was then incubated with preformed conventional liposomes or dilysocardiolipin liposomes for 1 hour at 37℃ and proteoliposome samples centrifuged at 100 000 g for 70 min to remove non-loaded proteins. To prepare artificial exosomes, palmitoylated Rab7, AHSG and Desmoplakin were combined and loaded together to dilysocardiolipin liposomes.

Data and Software Availability

The accession number for the proteomics data reported in this paper is EVPedia: 153144.

Both proteomics data and lipidomics data are available as Supplementary Tables 1 through 5.

Primary neuron culture

All animal procedures were approved by the University of Massachusetts Medical School Institutional Animal Care and Use Committee (IACUC, protocol number A-2411).

Primary cortical neurons were isolated from E15.5 mouse embryos of wild-type FVBNj mice. Pregnant females were anesthetized by intraperitoneal injection of Ketamine (100 mg/kg, KETASET®, *Zoetis, Kalamazoo, MI*) - Xylazine (10 mg/kg, AnaSed®, *AKORN, Laker Forest, IL, #NDC59399-111-50*) followed by cervical dislocation. Embryos were removed and transferred to ice-cold DMEM/F12 medium (*Invitrogen, Carlsbad, CA;* #11320). Brains were removed and meninges were carefully detached. Cortices were isolated and transferred into pre-warmed papain solution for 25 min at 37˚C, 5% CO_2 to dissolve the tissue. Papain (*Worthington, Lakewood, NJ;* #54N15251) was dissolved in 2 ml Hibernate E (*Brainbits, Springfield, IL;* #HE) and supplemented with 0.25 ml of 10 mg/ml DNase1 (*Worthington, Lakewood, NJ;* #54M15168) in Hibernate E. After 30 min incubation, the papain solution was removed and 1 ml NeuralQ (*Sigma-Aldrich, St. Louis, MO, #N3100*) supplemented with 2.5% FBS was added to the tissue. Tissues were then dissociated by trituration through a fire-polished, glass Pasteur pipet. Neurons were counted and diluted at 10^6 cells/ml. 10^5 neurons per well were plated on 96-well plates pre-coated with poly-L-lysine (*BD BIOCOAT, Corning, NY;* #356515). Neurons originating from all embryos (independently of gender) from one pregnant female were pooled, resulting in mixed-gender neuronal cultures. After overnight incubation at 37˚C, 5% CO_2, an equal volume of NeuralQ supplemented with anti-mitotics, 0.484 µl/ml of 5'UtP (*Sigma, St Louis, MO;* #U6625) and 0.2402 µl/ml of 5'FdU (*Sigma, St Louis, MO;* #F3503) was added to prevent the growth of

non-neuronal cells. Half of the volume of media was replaced with fresh NeuralQ containing anti-mitotic every 48 hours until the experiments were performed. Neurons were treated with siRNA-loaded EVs or liposomes (resuspended in NeuralQ medium) and incubated for 7 days at 37°C, 5% CO_2 post treatment.

Confocal microscopy

For the analysis of siRNA- loaded exosome uptake *in vitro*, primary neurons were plated in poly-L-lysine (*Sigma, St Louis, MO;* #P4707) coated 35 mm glass bottom dishes (*MatTek, Ashland, MA, #P35G-1.5-10-C*) were stained with NucBlue™ live cell stain (*Thermo Fisher Scientific, Waltham, MA, #R37605*) and neurons were treated with exosomes conatining fluorescently labeled siRNA targeting *Huntingtin* gene (Suppl. Table 1). Images were acquired with a Leica DM IRE2 (*Leica Microsystems Inc., Buffalo Grove, IL*) confocal microscope using a 40x oil-immersion objective and Dapi channel (exposure time 50 ms) as well as mCherry channel (exposure time 200 ms). Images were processed using ImageJ software[9] (*NIH, Bethesda, MD*). The relative uptake of siRNA, loaded in control exosomes or stressed exosomes, was estimated based on pixel integrated density of 5 images for each timepoint, and normalized to the number of nuclei per image (nuclei counted manually).

Mouse surgery

All animal procedures were approved by the University of Massachusetts Medical School Institutional Animal Care and Use Committee (IACUC, protocol number A-2411). ALZET® osmotic pumps (*ALZET Osmotic Pump, Cupertino, CA;* #1003D) were prefilled with 100 µl of sample following manufacturer instructions and primed overnight at 37°C in a water bath. Osmotic pumps were loaded with either PBS (100 µl per pump), or 6.6 x 10^{10} vesicles loaded with cholesterol-siRNA (3000 copies per vesicle, total dose 0.33 nmol) (100 µl per pump), or

equivalent amount of cholesterol-siRNA only (0.33 nmol, 100 µl per pump). Wild-type FVBNj (female, 7-10 weeks old) mice were deeply anesthetized with 1.2% Avertin (*Sigma, St Louis, MO;* #T48402). ALZET® osmotic pumps were then placed using a stereotactic device (*World Precision Instruments, Sarasota, FL, #502610*) into the right lateral ventricle (coordinates relative to bregma: 0.2 mm posterior, 0.8 mm lateral, 2.5 mm ventral). Pumps delivered their content for 3 days at 1 µl / hour rate. Mice were administered 4 mg/kg of meloxicam SR subcutaneously for pain management. Osmotic pumps were removed 5 days after infusion ended (8 days after placement) and wound closed with 7mm wound clips. Animals were euthanized 4 weeks after pump placement using isoflurane overdose. Brains were cut in 300 µm thick coronal sections at 4°C on a vibrotome, and 2 mm punches taken from striatum and motor cortex ipsilateral to the infusion. 3 punches were collected for mRNA quantification (immediately placed in RNAlater® (*Thermo Fisher Scientific, Waltham, MA, #AM7021*), and 3 punches were collected for protein quantification (immediately frozen in liquid nitrogen).

Measurement of mRNA levels

Primary neurons or brain punches were lysed in QuantiGene Lysis Mixture (part of QuantiGene Sample Processing Kit for cultured cells, *Affymetrix, Thermo Fisher Scientific, Waltham, MA, #QS0103*) or QuantiGene Homogenizing solution (*Affymetrix, Thermo Fisher Scientific, Waltham, MA, #QG0517*), respectively. mRNA quantification was performed using the QuantiGene 2.0 assay kit (*Affymetrix, Thermo Fisher Scientific, Waltham, MA,, #QS0103*)[10]. Catalog numbers for probes used in QuantiGene 2.0 assay were as follows: mouse *Htt* (Affymetrix, #SB-14150), mouse *Hprt* (Affymetrix, #SB-15463). Data sets were normalized to housekeeping gene *Hprt.*

Measurement of siRNA levels

siRNA guide strands in neuron cell lysates were quantified using a peptide-nucleic acid (PNA) hybridization assay [28-1,11-13]. PNAs are oligonucleotides, where the sugar-phosphate backbone is replaced with a charge-neutral polyamide backbone. PNAs have therefore a high hybridization energy to RNA. SDS from leftover neuron lysates after mRNA quantification was precipitated with 3 M KCl and pelleted at 4,000 × *g* for 15 min. siRNA guide strands in cleared supernatant were hybridized to fully complementary Cy3-labeled PNA strands (*PNABio, Thousand Oaks, CA*). siRNA guide strand-PNA duplexes were injected into HPLC DNAPac® PA100 anion exchange column (*Thermo Scientific, Carlsbad, CA*) and Cy3 fluorescence was monitored and peaks integrated. The mobile phase for HPLC was 50% water 50% acetonitrile, 25 mM Tris-HCl (pH 8.5), 1 mM EDTA and the salt gradient was 0 to 800 mM $NaClO_4$. For the calibration curve, a known amount of siRNA duplex was spiked into cell lysis solution.

Statistical Analysis

siRNA uptake, mRNA silencing, cell viability, and Lipidomics data were analyzed using GraphPad Prism 7, version 7.04 (*GraphPad Software Inc., La Jolla, CA*). In *in vitro* siRNA uptake experiments curves were fitted using "exponential growth equation" (PNA hybridization assay data) or "one phase association" (confocal microscopy data). In *in vitro* silencing experiments dose-response curves were fitted using "log(inhibitor) *vs.* response – variable slope (three parameters)" equation. Curves were compared using two-way ANOVA with Tukey multiple comparison for main column effect. In *in vivo* silencing experiments and cell viability assay groups were compared using one-way ANOVA with Tukey multiple comparison test. When comparing candidate proteins between control and stressed conditions two-way ANOVA

with multiple comparison for row effect according to the original FDR method of Benjamini and Hochberg. During lipidomics the amount of lipids were normalized to protein content of samples. Lipid classes in control *versus* stressed EVs or cells were compared using two-way ANOVA with Tukey multiple comparison for compare rows within columns. Fatty acid tail properties were correlated with enrichment score using linear regression.

Label-free quantification of proteins was performed *via* the iBAQ (intensity-based absolute quantification[14]) method in Scaffold Viewer (Proteome Software Inc.). Briefly, this method normalizes signal to the number of tryptic sites in a protein. Gene Ontology was performed using DAVID version 6.7 [15,16] (NIH). Volcano plots and heatmaps were generated in R^2 using "ggplot2" and "pheatmap" packages.

Differences in all comparisons were considered significant at p-values < 0.05.

1 Haraszti, R. A. *et al.* 5-Vinylphosphonate improves tissue accumulation and efficacy of conjugated siRNAs in vivo. *Nucleic Acids Res* **45**, 7581-7592 (2017).

2 Didiot, M.-C. *et al.* Exosome-mediated Delivery of Hydrophobically Modified siRNA for Huntingtin mRNA Silencing. *Molecular Therapy*, doi:10.1038/mt.2016.126 (2016).

3 Didiot, M. C. *et al.* Exosome-mediated delivery of hydrophobically modified siRNA for Huntingtin mRNA silencing. *Molecular Therapy* **24**, 1836-1847 (2016).

4 Haraszti, R. A. *et al.* Exosomes Produced from 3D Cultures of MSCs by Tangential Flow Filtration Show Higher Yield and Improved Activity. *Mol Ther* **22**, 30456-30458 (2018).

5 Haraszti, R. A. *et al.* High-resolution proteomic and lipidomic analysis of exosomes and microvesicles from different cell sources. *J Extracell Vesicles* **5**, 32570 (2016).

6 Haraszti, R. A. D., Marie-Cecile; Sapp, Ellen; Leszyk, John; Shaffer, Scott A ; Rockwell, Hannah E; Gao, Fei; Narain, Niven R; DiFiglia, Marian; Kiebish, Michael A; Aronin, Neil; Khvorova, Anastasia High-resolution proteomic and lipidomic analysis of exosomes and microvesicles from different cell sources. . *Journal of Exrtacellular Vesicles* **In press** (2016).

7 Kiebish, M. A. *et al.* Dynamic simulation of cardiolipin remodeling: greasing the wheels for an interpretative approach to lipidomics. *J Lipid Res* **51**, 2153-2170 (2010).

8 Simons, B. *et al.* Shotgun Lipidomics by Sequential Precursor Ion Fragmentation on a Hybrid Quadrupole Time-of-Flight Mass Spectrometer. *Metabolites* **2**, 195-213 (2012).

9 Schneider, C. A., Rasband, W. S. & Eliceiri, K. W. NIH Image to ImageJ: 25 years of image analysis. *Nat Methods* **9**, 671-675 (2012).

10 Coles, A. H. *et al.* A High-Throughput Method for Direct Detection of Therapeutic Oligonucleotide-Induced Gene Silencing In Vivo. *Nucleic Acid Ther* **26**, 86-92 (2016).
11 Nikan, M. *et al.* Synthesis and evaluation of parenchymal retention and efficacy of a metabolically stable O-Phosphocholine-N-docosahexaenoyl-l-serine siRNA conjugate in mouse brain. *Bioconjugate Chem.* **28**, 1758-1766 (2017).
12 Nikan, M. *et al.* Docosahexaenoic Acid Conjugation Enhances Distribution and Safety of siRNA upon Local Administration in Mouse Brain. *Mol Ther Nucleic Acids* **5**, e344, doi:10.1038/mtna.2016.50 (2016).
13 Roehl, I., Schuster, M. & Seiffert, S. Vol. US20110201006 A1 (2011).
14 Wilhelm, M. *et al.* Mass-spectrometry-based draft of the human proteome. *Nature* **509**, 582-587 (2014).
15 Huang da, W., Sherman, B. T. & Lempicki, R. A. Bioinformatics enrichment tools: paths toward the comprehensive functional analysis of large gene lists. *Nucleic Acids Res* **37**, 1-13 (2009).
16 Huang da, W., Sherman, B. T. & Lempicki, R. A. Systematic and integrative analysis of large gene lists using DAVID bioinformatics resources. *Nat Protoc* **4**, 44-57 (2009).